Available online at www.sciencedirect.com

ScienceDirect

Geochimica et Cosmochimica Acta 206 (2017) 273–295

Geochimica et Cosmochimica Acta

www.elsevier.com/locate/gca

Trace element partitioning between plagioclase and silicate melt: The importance of temperature and plagioclase composition, with implications for terrestrial and lunar magmatism

Chenguang Sun [a,b,*], Michelle Graff [a], Yan Liang [a]

[a] Department of Earth, Environmental and Planetary Sciences, Brown University, Box 1846, Providence, RI 02912, USA
[b] Department of Geology and Geophysics, Woods Hole Oceanographic Institution, Woods Hole, MA 02543, USA

Received 30 April 2016; accepted in revised form 1 March 2017; available online 9 March 2017

Abstract

Trace element partition coefficients between anorthitic plagioclase and basaltic melts (D) have been determined experimentally at 0.6 GPa and 1350–1400 °C in a lunar high-Ti picritic glass and a mid-ocean ridge basalt (MORB). Plagioclases with 98 mol% and 86 mol% anorthite were produced in the lunar picritic melt and MORB melt, respectively. Based on the new experimental partitioning data and those selected from the literature, we developed parameterized lattice strain models for the partitioning of monovalent (Na, K, Li), divalent (Ca, Mg, Ba, Sr, Ra) and trivalent (REE and Y) cations between plagioclase and silicate melt. Through the new models we showed that the partitioning of these trace elements in plagioclase depends on temperature, pressure, and the abundances of Ca and Na in plagioclase. Particularly, Na content in plagioclase primarily controls divalent element partitioning, while temperature and Ca content in plagioclase are the dominant factors for REE partitioning in plagioclase. From these models, we also derived a new expression for D_{Ra}/D_{Ba} that can be used for Ra-Th dating on volcanic plagioclase phenocrysts, and a new model for plagioclase-melt noble gas partitioning. Applications of these partitioning models to fractional crystallization of MORB and lunar magma ocean (LMO) indicate that (1) the competing effect of temperature and plagioclase composition leads to small variations of plagioclase-melt D_{REE} during MORB differentiation, but (2) the temperature effect is especially significant and can vary anorthite-melt D_{REE} by over one order of magnitude during LMO solidification. Temperature and plagioclase composition have to be considered when modeling the chemical differentiation of mafic to felsic magmas involving plagioclase.

Keywords: Partition coefficient; Trace element; Noble gas; Plagioclase; Lunar ferroan anorthosite; Mid-ocean ridge basalt

1. INTRODUCTION

Plagioclase is one of the major rock-forming minerals constituting the crusts of Earth and the Moon. As a low-pressure liquidus phase that crystallizes over a wide range of temperature, plagioclase is often present as a phenocryst in volcanic rocks or as a cumulus phase in mafic to felsic intrusions. Gabbros, the principal rocks in lower oceanic crust, solidify from mid-ocean ridge basalts (MORB) and contain abundant plagioclases (>~40 vol%) with a broad range of anorthite content (~50–90 mol%; e.g., Dick et al., 2000; Lissenberg et al., 2013). The dominant rocks in the lunar crust are ferroan anorthosites (FANs) and Mg-suite rocks (mostly norite and troctolite). Mg-suite

* Corresponding author at: Department of Earth Science, Rice University, 6100 Main Street, MS-126, Houston, TX 77005, USA.
E-mail address: csun@rice.edu (C. Sun).

http://dx.doi.org/10.1016/j.gca.2017.03.003
0016-7037/

rocks have ~15–90 vol% plagioclase with ~67–97 mol% anorthite (Shearer et al., 2015; and references therein), while FANs are characterized by >90 vol% anorthite plagioclases (anorthite >95 mol%; e.g., McGee, 1993; Papike et al., 1998; Gross et al., 2014). According to the canonic models of lunar formation and evolution, FANs are a consequence of crystallization and floatation of plagioclase in a global-scale magma ocean (e.g., Wood et al., 1970; Smith et al., 1970; Warren, 1985; Snyder et al., 1992). Thus, plagioclase crystallization can significantly fractionate trace elements during differentiation of terrestrial and lunar magmas.

A key parameter for unraveling magmatic processes involving plagioclase is the plagioclase-melt trace element partition coefficient (D), which generally is a function of temperature, pressure, and compositions of the mineral and melt (e.g., Wood and Blundy, 2003; and references therein). Since the pioneering work of Drake and Weill (1975), many experimental studies have been conducted to determine trace element partitioning between plagioclase and silicate melt (e.g., McKay, 1982; Blundy and Wood, 1994; Peters et al., 1995; Blundy, 1997; Blundy et al., 1998; Bindeman et al., 1998; Bindeman and Davis, 2000; Miller et al., 2006, 2007; Aigner-Torres et al., 2007; Fabbrizio et al., 2009; Tepley et al., 2010; de Vries et al., 2012; Laubier et al., 2014; Dohmen and Blundy, 2014). However, anorthite-melt trace element partition coefficients have not yet been systematically investigated for lunar-relevant melt compositions and temperatures. To estimate rare earth element (REE) abundances in the parent magmas of FANs and Mg-suite rocks, previous geochemical studies on lunar cumulate samples (e.g., Papike et al., 1996, 1997; Floss et al., 1998; Shervais and McGee, 1998) used the anorthite-melt Eu partition coefficients from Jones (1995) or Weill and McKay (1975) and the REE partition coefficients between anorthite megacrysts and coexisting matrices from Phinney and Morrison (1990). Although several models have been calibrated for predicting plagioclase-melt REE partition coefficients (e.g., Blundy and Wood, 1991; Bindeman et al., 1998; Bindeman and Davis, 2000; Wood and Blundy, 2003; Bédard, 2006; Tepley et al., 2010; Hui et al., 2011; Dohmen and Blundy, 2014), these models are still not able to reproduce many of recent experimental data (see Fig. 1 and Section 2).

In this study, we experimentally determine trace element partition coefficients between anorthite and a lunar basaltic melt and between anorthitic plagioclase and a MORB melt. Based on the experimental data from this study and those reported in the literature, we develop new parameterized lattice strain models for the partitioning of monovalent (Na^+, K^+, Li^+), divalent (Ca^{2+}, Mg^{2+}, Sr^{2+}, Ba^{2+}, Ra^{2+}), and trivalent (REE^{3+}, Y^{3+}) cations between plagioclase and silicate melt. We show that these generalized partitioning models are significantly improved over previous models and can be used (1) to estimate the relative partitioning of Ra and Ba for Ra-Th dating on volcanic plagioclase phenocrysts, (2) to constrain noble gas partitioning in plagioclase, and (3) to better assess trace element fractionation during crystallization of terrestrial and lunar magmas.

2. PREVIOUS PLAGIOCLASE-MELT PARTITIONING MODELS

2.1. Log-linear formulations

Through a comprehensive compilation of the published Sr and Ba partitioning data from laboratory experiments and natural samples, Blundy and Wood (1991) showed that trace element partition coefficients between plagioclase and silicate melt are inversely correlated with anorthite content in plagioclase and can be described by a log-linear expression

$$RT \ln D_j = a \times An + b, \quad (1)$$

where D_j is the plagioclase-melt partition coefficient of element j; R is the gas constant; An is the anorthite content in plagioclase ($An = 100 \times Ca/(Ca + Na + K)$, in mole); T is the temperature in K; and a and b are constant coefficients. Eq. (1) suggests that both crystal chemistry and temperature are important factors controlling trace element partitioning between plagioclase and silicate melt.

Several studies further calibrated Eq. (1) for a more complete set of trace elements against experimentally determined partitioning data (e.g., Bindeman et al., 1998; Tepley et al., 2010; Hui et al., 2011), or against partitioning data from both laboratory experiments and natural samples (Bédard, 2006). To test the accuracy of these published models, we compared the partition coefficients of REE + Y derived from these models with those reported in recent experimental studies (Blundy et al., 1998; Bindeman et al., 1998; Bindeman and Davis, 2000; Aigner-Torres et al., 2007; Tepley et al., 2010; and two experiments from the present study). To facilitate comparison, we calculated the Pearson's Chi-square (χ^2_p) for each model using the expression

$$\chi^2_p = \sum_{j=1}^{N} \frac{(D_j - D_j^m)^2}{D_j}, \quad (2)$$

where N is the total number of plagioclase-melt partitioning data; D_j^m is the measured partition coefficients for element j; and D_j is the partition coefficient predicted by the model. χ^2_p is a measure of the relative offset of the predictions from the measured values: a smaller χ^2_p indicates a better predictive model. Fig. 1a–c shows that these models yield large χ^2_p values (2.6–8.5) and fail to reproduce a significant amount of REE partition coefficients. The apparent uncertainties of these models suggest that the simple log-linear expression (Eq. (1)) cannot fully characterize trace element, particularly REE and Y, partitioning in plagioclase.

2.2. Lattice Strain Models

The partition coefficients of isovalent cations from a given mineral-melt partitioning experiment vary systematically with their ionic radii in the Onuma diagram (partition coefficients vs. ionic radii; Onuma et al., 1968). When multiple isovalent cations all partition into the same lattice site of the crystal, their partition coefficients form a near-parabolic pattern in the Onuma diagram that can be quan-

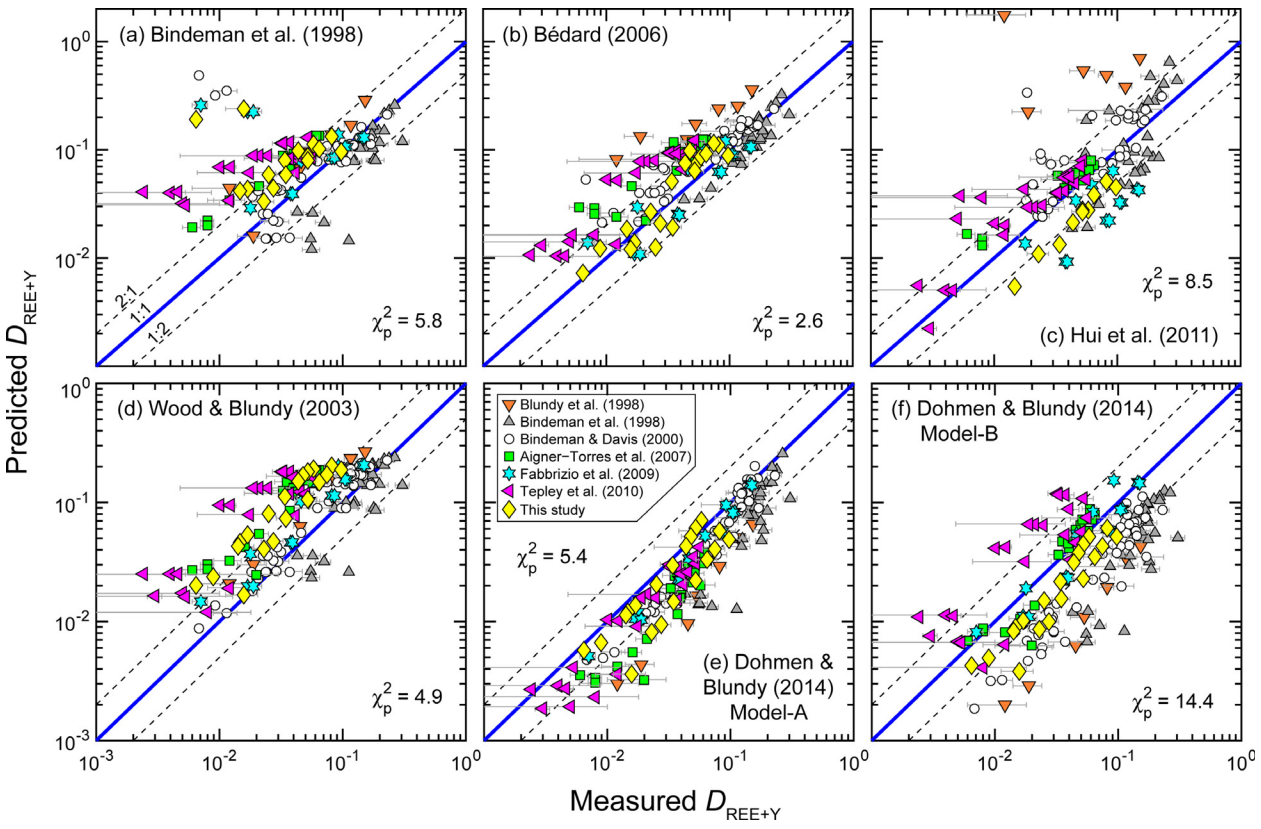

Fig. 1. Comparisons of experimentally determined and model predicted plagioclase-melt REE + Y partition coefficients (D_{REE+Y}). Solid lines are 1:1 lines, and dashed lines are 1:2 and 2:1 lines. Error bars are 1σ errors of the measured partitioning data. χ_p^2 is the Pearson's Chi-square as defined by Eq. (2) to aid model evaluation. Note that the predicted partition coefficients were calculated using the original models cited in the plots. See Supplementary Fig. S2 for details of individual experiments.

titatively described by the lattice strain model (Brice, 1975; Blundy and Wood, 1994),

$$D_j = D_0 \exp\left[\frac{-4\pi E N_A}{RT}\left(\frac{r_0}{2}(r_0 - r_j)^2 - \frac{1}{3}(r_0 - r_j)^3\right)\right], \quad (3)$$

where D_0 is the strain-free partition coefficient; r_j is the ionic radius of element j; r_0 is the ionic radius of the strain-free lattice site; E is the effective Young's modulus; and N_A is Avogadro constant. A generalized model may be obtained by further parameterizing the three lattice strain parameters (D_0, r_0, and E) as a function of temperature, pressure and composition.

Wood and Blundy (2003) proposed preliminary lattice strain models for plagioclase-melt trace element partitioning based on the experimental trace element partitioning data of Bindeman et al. (1998) and Bindeman and Davis (2000). Using Na, Ca, and La partition coefficients as references, Wood and Blundy (2003) eliminated the strain-free partition coefficient (D_0) in the lattice strain model for 1+, 2+, and 3+ cations, respectively. They suggested that the apparent Young's modulus is a constant and that the ionic radius of the ideal cation (r_0) decreases linearly with An in plagioclase. Their normalized model, however, significantly overestimates the more recent experimental REE partition coefficients for high-An plagioclase by up to one order of magnitude (Fig. 1d). This may be attributed to uncertainties in the underconstrained lattice strain parameters (E and r_0) in Wood and Blundy's original model and the log-linear expression of La partitioning model (Eq. (1); see also Fig. 1c).

Following the approach of Wood and Blundy (2003), Dohmen and Blundy (2014) developed new normalized lattice strain models for plagioclase-melt partitioning of 1+, 2+, and 3+ trace cations using Na, Ca, and La partition coefficients as references, respectively. Based solely on their new experimental data, they described both E and r_0 as a linear function of An in plagioclase and parameterized D_{La} as a function of temperature, D_{Ca}, and D_{Na}. However, application of their initial model requires knowledge of Ca and Na contents in both plagioclase and equilibrium melt, which are usually not available in plagioclase-bearing rocks (e.g., gabbros, norites, and anorthosites). To develop a generalized model, they further parameterized D_{Ca} and D_{Na} as functions of temperature, SiO_2 content in the melt, and An in plagioclase. For REE and Y, their initial model ($\chi_p^2 = 5.4$; Fig. 1e) better reproduces the literature experimental partitioning data than their generalized model ($\chi_p^2 = 14.4$; Fig. 1f) but still systematically underestimates the literature data of middle and heavy REE by up to a factor of six.

The significant discrepancies between model-predicted partitioning data and the experimentally determined values

($\chi^2_p = 2.6$–14.4; Fig. 1a–f) demonstrate the need of additional modeling to better characterize the experimentally determined plagioclase-melt REE + Y partition coefficients. As shown in Supplementary Fig. S1, a similar statement can be made for the partitioning of monovalent (Na, K, Li, Rb) and divalent (Ca, Mg, Sr, Ba, Ra) cations in plagioclase. Here we follow a procedure that has been successfully used to develop parameterized lattices strain models for REE + Y partitioning between major rock-forming minerals (clinopyroxene, orthopyroxene, garnet, and olivine) and basaltic melts (Sun and Liang, 2012, 2013a, 2013b; Yao et al., 2012; Dygert et al., 2014) by fitting all three lattice-strain parameters (D_0, E, and r_0) as a function of temperature, pressure and composition using experimentally determined plagioclase-melt partition coefficients reported in the literature. Since trace partitioning data for anorthite-melt systems are limited, we supplement the published data by two additional experiments detailed below.

3. PLAGIOCLASE-MELT PARTITIONING EXPERIMENTS

3.1. Experimental methods and results

The experimental studies in the literature on plagioclase-melt trace element partitioning mainly focused on plagioclases with intermediate anorthite content at 1 atm. To further expand the existing data, we conducted two piston-cylinder experiments at 0.6 GPa using two starting compositions, a synthetic Apollo 15 red glass (A15Red) and a primitive mid-ocean ridge basalt (MORB) glass. The two experiments were held at 1400 °C for 36 h and at 1350 °C for 50 h, respectively. Both experiments produced large plagioclase crystals (~80–400 μm) evenly distributed in abundant quenched melts (Fig. 2). Plagioclase crystals are euhedral without zoning, and the quenched melts are clear without dendritic quench textures. Major and trace element compositions of plagioclase and melt from the two experiments were determined using the electron microprobe and LA-ICP-MS, respectively. Details of the experimental method and starting composition are presented in online Supplementary Materials (Section S1 and Table S1). Experimental run conditions and run products are summarized in Table 1. Individual analyses for major and trace elements are presented in Supplementary Tables S2 and S3.

Small standard deviations in averaged major and trace element compositions suggest a homogeneous melt composition in each run. The melt from run An-Red-2 is high in TiO_2 (6.44 wt%) and low in SiO_2 (41.82 wt%) with intermediate Mg# (= 49; Mg# = 100 × Mg/(Mg + Fe), in mole). The melt from run An-MORB-2 is low in TiO_2 (1.20 wt %) and slightly higher in SiO_2 (46.20 wt%) with a higher Mg# (= 64). Plagioclase crystals are anorthitic (An = 98 for An-Red-2, and An = 86 for An-MORB-2). The Ca-Na exchange coefficient between plagioclase (plg) and melt ($K_D = (Ca/Na)_{plg}/(Ca/Na)_{melt}$) are 1.2 and 1.3 for runs An-Red-2 and An-MORB-2, respectively, comparable with those (0.7–2.7) from recent partitioning studies (Blundy, 1997; Aigner-Torres et al., 2007; Bindeman et al., 1998; Bindeman and Davis, 2000; Tepley et al., 2010). A number

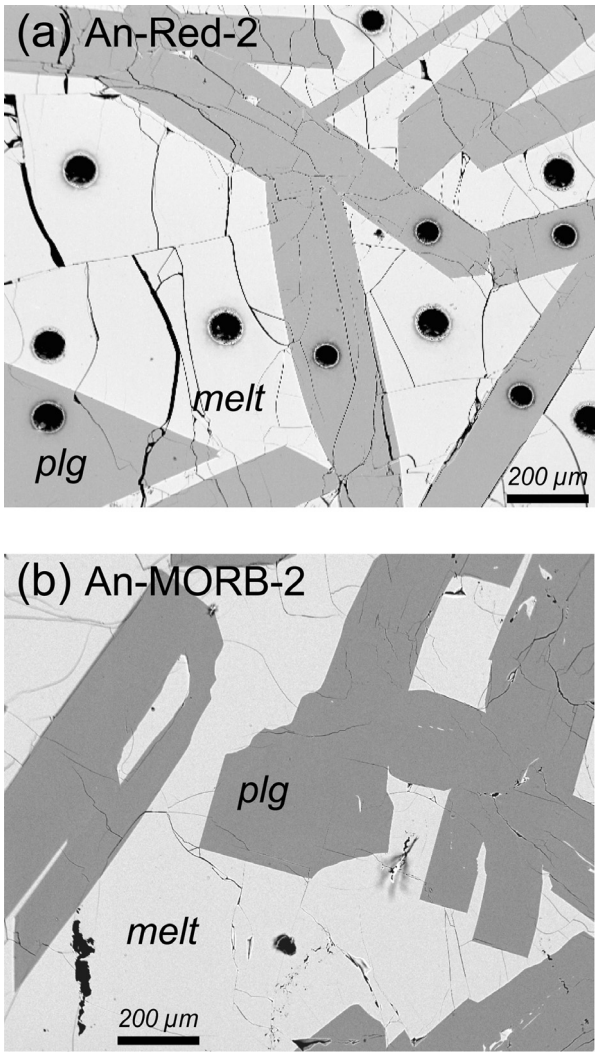

Fig. 2. Back-scattered electron images of experimental products of runs An-Red-2 (a) and An-MORB-2 (b). *plg* stands for plagioclase. Round black holes in (a) are laser ablation spots.

of undoped trace elements (Li, Sr, Ba, P, Sc, V, Co, Ni, Cu, Zn, Mo, Pb, Th, and U) are present at detectable levels with small standard deviations (Table 1). These were likely derived from the natural MORB glass used in run An-MORB-2 and/or possibly introduced as impurities in the doped trace element oxides.

Plagioclase-melt partition coefficients are calculated according to the element concentration ratios by weight in plagioclase and coexisting melt. The partitioning data are reported in Table 1 and compared with the literature data in Fig. 3. Our new partitioning experiments provide the first Mo and W partition coefficients between plagioclase and silicate melt, which differs by one or two orders of magnitude between runs An-Red-2 and An-MORB-2. In general, our trace element partition coefficients are within the literature range, except those of high field strength elements (HFSE: Hf, Zr, Nb, and Ta) from run An-Red-2 that are significantly less than the literature values and are about one to two orders of magnitude smaller

than those from run An-MORB-2. The partition coefficients of Li, K, Sr, Eu, and Pb between these two runs are nearly identical, while REE partition coefficients from run An-Red-2 are less than those from An-MORB-2 by up to a factor of three. As run An-Red-2 started from a Ti-rich composition and produced more anorthitic plagio-

Table 1
Experimental run products and partition coefficients.

Run #	An-Red-2			An-MORB-2		
Starting material	66% An+ 34% A15Red			25% An+ 75% MORB		
Run condition	1400 °C/6 kbar			1350 °C/6 kbar		
T-t path[a]	1450 (0.5)/1/1400(36)			1450 (0.5)/0.5/1350(50)		
Phase	Plagioclase	Melt	D[b]	Plagioclase	Melt	D
EMP[c]	N[d] = 15	$N = 10$		$N = 10$	$N = 8$	
SiO_2 (wt%)	43.29(26)[e]	41.82(32)	1.04(1)	46.84(50)	46.5(6)	1.01(2)
TiO_2	0.13(2)	6.44(23)	0.020(3)	0.03(1)	1.2(0)	0.023(7)
Al_2O_3	35.91(18)	22.2(3)	1.62(3)	34.77(43)	19.13(30)	1.82(4)
Cr_2O_3		0.27(4)			0.01(2)	
FeO	0.18(8)	10(0.17)	0.018(8)	0.14(1)	8.97(20)	0.015(2)
MnO		0.17(2)			0.16(2)	
MgO	0.15(2)	5.49(9)	0.028(4)	0.22(1)	9.11(21)	0.024(2)
CaO	18.78(20)	10.44(17)	1.799(35)	17.25(41)	12.39(7)	1.39(3)
Na_2O	0.18(4)	0.12(2)	1.465(401)	1.58(22)	1.48(9)	1.07(16)
K_2O	0.02(1)	0.11(1)	0.20(7)	0.01(0)	0.07(0)	0.17(5)
P_2O_5		0.04(3)				
Total	98.64(44)	97.11(50)		100.84(20)	99.03(25)	
An/Mg#[f]	98.16	49.46		85.70	64.43	
LA-ICP-MS	$N = 9$	$N = 10$		$N = 8$	$N = 7$	
Al_2O_3 (wt%)	33.7(7)	21.7(5)	1.56(5)	33 (1)	19.14(44)	1.72(7)
TiO_2	0.122(5)	6.63(33)	0.018(1)	0.082(23)	1.216(25)	0.067(19)
Na_2O	0.13(1)	0.094(2)	1.36(8)			
MgO	0.15(1)	5.14(15)	0.030(3)	0.59(18)	9.29(25)	0.063(19)
FeO	0.163(11)	10.00(33)	0.016(1)	0.59(22)	9.27(26)	0.064(24)
MnO	0.008(1)	0.158(2)	0.052(5)	0.013(3)	0.166(4)	0.078(21)
P_2O_5	0.009(1)	0.030(2)	0.284(37)		0.093(7)	
K_2O	0.014(2)	0.090(3)	0.151(17)	0.012(1)	0.062(3)	0.186(17)
Li (ppm)	3.86(28)	11.86(28)	0.33(2)	2.93(37)	13.43(35)	0.22(3)
Sc	4.16(20)	4.11(13)	1.01(6)	12.70(89)	37(1)	0.34(3)
V		4.48(22)		23(7)	254(11)	0.09(3)
Cr	35(1)	1722(345)	0.020(4)	26(10)	398(17)	0.064(26)
Co	0.057(6)	2.95(8)	0.019(2)	3.1(6)	36(1)	0.086(18)
Ni	0.96(0.00)	11(1)	0.09(1)	11.41(0.00)	21(4)	0.55(11)
Cu	1.54(16)	18(2)	0.08(1)	11(5)	81(12)	0.14(6)
Zn	0.99(15)	52(2)	0.019(3)	8(2)	101(4)	0.082(23)
Sr	51(1)	38.22(78)	1.33(5)	74(2)	53(1)	1.39(5)
Y	7.48(33)	512(32)	0.015(1)	25(5)	1064(26)	0.023(5)
Zr	0.121(18)	555(40)	0.00022(4)	16(8)	1047(24)	0.015(7)
Nb	0.14(2)	459(24)	0.00032(5)	41(17)	920(18)	0.044(19)
Mo	0.20(8)	15(3)	0.013(6)	14(4)	179(53)	0.079(33)
Cs		4.5(3)		0.200(17)	4.2(9)	0.047(11)
Ba	2.32(37)	21.1(8)	0.110(18)	2.69(52)	15(1)	0.176(36)
La	25(2)	433(22)	0.058(5)	69(8)	856(20)	0.081(10)
Ce	22(1)	429(23)	0.0524(41)	91(21)	929(23)	0.098(22)
Pr	20(1)	425(25)	0.0476(36)	68(14)	906(26)	0.075(15)
Nd	18.1(8)	414(24)	0.0437(32)	55(10)	846(25)	0.065(13)
Sm	13.82(64)	408(23)	0.0339(25)	48(9)	915(28)	0.052(10)
Eu	174(10)	323(10)	0.538(36)	371(14)	596(8)	0.622(25)
Gd	12.44(41)	497(31)	0.0250(17)	35(6)	1019(25)	0.0348(58)
Dy	8.73(39)	520(33)	0.0168(13)	28(6)	1037(29)	0.0273(55)
Ho	6.21(25)	439(24)	0.0141(10)	23(4)	1041(28)	0.0225(40)
Yb	3.91(19)	441(27)	0.0089(7)	24(7)	1088(28)	0.0222(69)
Lu	2.80(18)	434(26)	0.00646(57)	17(5)	1081(23)	0.0158(46)
Hf	0.123(28)	501(41)	0.000246(60)	12(5)	953(61)	0.0127(57)
Ta	0.112(17)	407(26)	0.000275(45)	20(9)	855(46)	0.023(10)
W	0.049(29)	391(22)	0.000125(73)	54(28)	874(26)	0.062(33)

(*continued on next page*)

Table 1 (*continued*)

Run #	An-Red-2			An-MORB-2		
Starting material	66% An+ 34% A15Red			25% An+ 75% MORB		
Run condition	1400 °C/6 kbar			1350 °C/6 kbar		
T-t path[a]	1450 (0.5)/1/1400(36)			1450 (0.5)/0.5/1350(50)		
Phase	Plagioclase	Melt	D[b]	Plagioclase	Melt	D
Pb	0.97(9)	9.54(28)	0.102(10)	1.21(19)	9.03(26)	0.134(21)
Th	0.0015(8)	1.59(12)	0.00091(53)	0.018(13)	0.82(7)	0.022(16)
U	0.00082(34)	1.46(8)	0.00056(23)	0.098(50)	1.40(10)	0.070(36)

[a] T-t path is the temperature-time path of the experimental run. 1450(0.5)/1/1400(36) follows $T_{initial}$(duration)/cooling rate (°C/min)/T_{final}(duration), where $T_{initial}$ is the initial temperature in °C, T_{final} is the final run temperature in °C, and duration is in hour.
[b] D is the partition coefficient calculated by taking the ratio of the element concentrations in the plagioclase and in the melt.
[c] Electron microprobe analyses.
[d] Numbers of spot analyses.
[e] Numbers in parentheses are one standard deviation (1σ) of replicate analyses in terms of last significant numbers; 43.29(26) should be read as 43.29 ± 0.26.
[f] An $= 100 \times$ Ca/(Ca + Na + K) in mole for the plagioclase; Mg# $= 100 \times$ Mg/(Mg + Fe) in mole for the melt.

clase at higher temperature, the discrepancies of trace element partition coefficients between runs An-Red-2 and An-MORB-2 highlight the importance of temperature and/or composition on trace element partitioning in plagioclase.

Compared with those from Phinney and Morrison (1990; $D_{Ce} = 0.03$, $D_{Sc} = 0.007$, $D_{Ba} = 0.8$, $D_{Th} = 0.02$), REE partition coefficients from run An-Red-2 are about a factor of two greater, Sc partition coefficient is two orders of magnitude larger, and Ba and Th partition coefficients are about one order of magnitude smaller. The differences between our experimental partitioning data for a lunar relevant composition (run An-Red-2) and those from Phinney and Morrison (1990) suggest that the latter partitioning data likely introduce systematic errors when used to estimate the parent magma compositions of FANs and Mg-suite rocks.

3.2. Site occupancies and lattice strain fits

The structure of plagioclase crystals follows a general formula MT_4O_8, where the M site contains larger cations (e.g., Ca^{2+} and Na^{+}) in VII- to IX-fold coordination, and the T site contains tetrahedrally coordinated smaller cations (Si^{4+} and Al^{3+}). Because REE^{3+}, Ca^{2+} and Na^{+} have similar ionic radii (REE^{3+}: 0.977–1.16 Å; Ca^{2+}: 1.12 Å; Na^{+}: 1.18 Å; VIII-fold coordination; Shannon, 1976), REE enter the M site in plagioclase by substituting for Ca^{2+} or Na^{+}. This substitution is likely charge balanced by Na^{+} replacing Ca^{2+} in the M site (Kneip and Liebau, 1994; Dohmen and

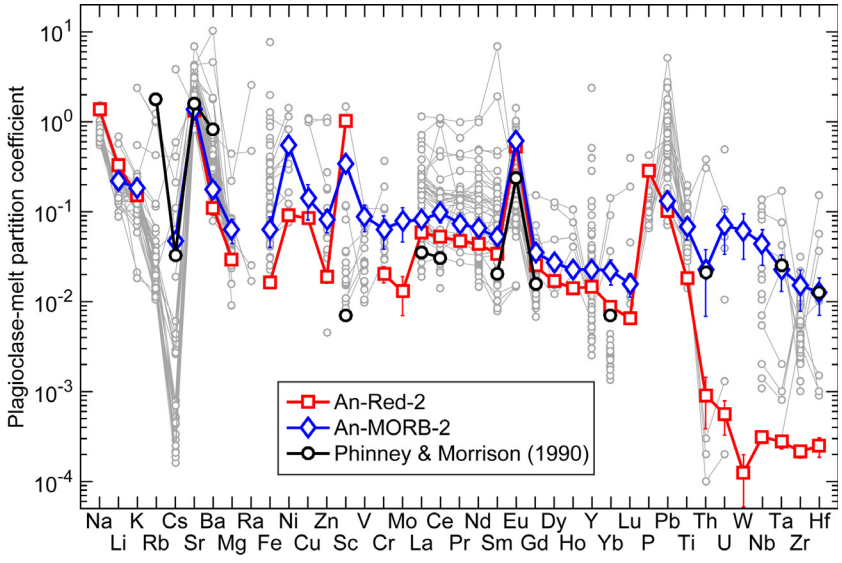

Fig. 3. Spider diagram showing experimentally determined plagioclase-melt trace element partition coefficients in this study and those from the literature. The gray lines with circle markers display the partitioning data from Blundy (1997), Blundy et al. (1998), Bindeman et al. (1998), Bindeman and Davis (2000), Miller et al. (2006, 2007), Aigner-Torres et al. (2007), Fabbrizio et al. (2009), Tepley et al. (2010), Laubier et al. (2014), and Dohmen and Blundy (2014). Error bars represent one standard deviation of measured partitioning data from this study. The phenocryst-matrix partition coefficients from Phinney and Morrison (1990) are shown as black lines with circle markers.

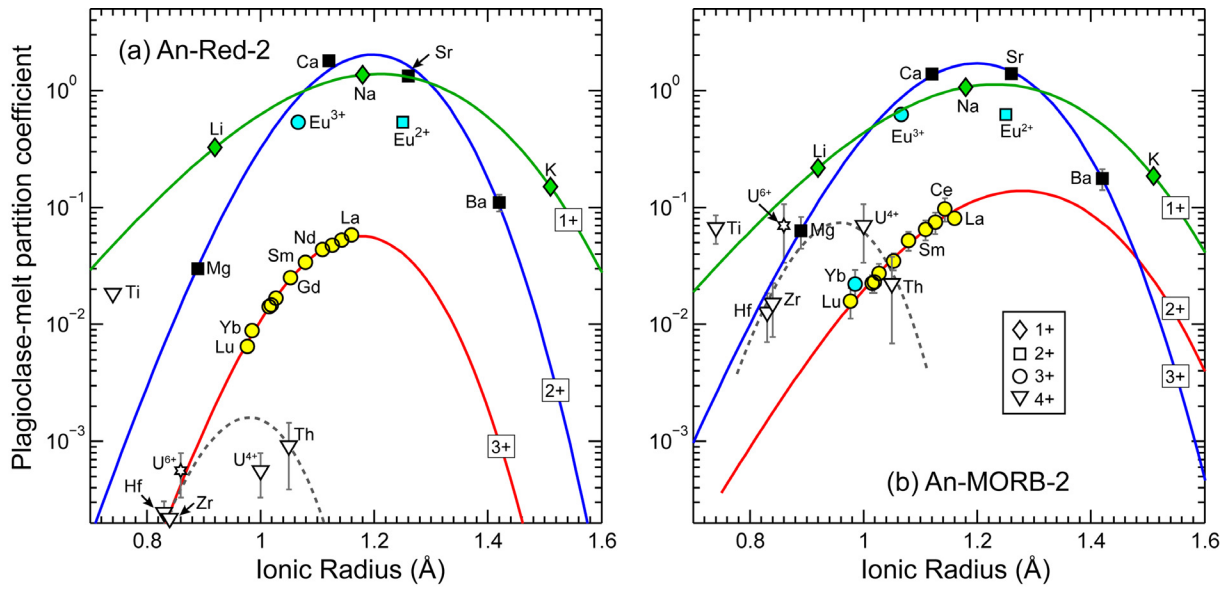

Fig. 4. Onuma diagrams showing the measured plagioclase-melt partition coefficients for monovalent, divalent, and trivalent elements as a function of the ionic radius. The partitioning data are from runs An-Red-2 (a) and An-MORB-2 (b) reported in this study. Solid curves are the best fits to the measured partition coefficients using the lattice strain model (Eq. (3)). Eu partition coefficients are not included in the fits, and Yb partition coefficient from run An-MORB-2 is also excluded. Eight-fold coordinated ionic radii from Shannon (1976) are used in the lattice strain model. The inverted lattice strain parameters are listed in Table 2.

Blundy, 2014). Monovalent Li^+, K^+, and Rb^+ are believed to replace Na^+, while divalent Sr^{2+}, Eu^{2+}, and Ba^{2+} likely substitute for Ca^{2+} in plagioclase (e.g., Blundy and Wood, 1994). It has also been suggested that smaller divalent cations such as Mg^{2+} may enter both the M and T sites (e.g., Longhi et al., 1976; Miller et al., 2006). Because of their very small ionic radii, tetravalent cations Ti^{4+} (0.42 Å), Hf^{4+} (0.58 Å), and Zr^{4+} (0.59 Å, IV-fold coordination; Shannon, 1976) have been suggested to preferentially enter the T site (e.g., Peters et al., 1995; Bindeman et al., 1998; Aigner-Torres et al., 2007); however, recently de Vries et al. (2012) suggested that similar to Th^{4+} and U^{4+}, Hf^{4+} and Zr^{4+} may enter the M site.

Fig. 4 displays our new partition coefficients of four groups of cations (1+, 2+, 3+, and 4+) in Onuma diagrams. Because of the complications of crystal-field effects on the first row transition metals (e.g., V, Cr, Mn, Fe, Co, Ni, Cu) as well as their multivalent states, no attempt is made here to examine the parabolic relationship between their partition coefficients and ionic radii in Onuma diagrams. For each of our experiments, monovalent, divalent, and trivalent cations fall on three different parabolas with similar peak positions (r_0), indicating that they all (including Mg^{2+}) enter the M site in plagioclase. REE partition coefficients are systematically smaller than those of monovalent and divalent cations. Eu falls between the two parabolas defined by the divalent and trivalent cations in the Onuma diagram, suggesting that it is present as both 2+ and 3+ cations. The Yb partition coefficient from run An-MORB-2 is slightly above the parabola defined by REE, which may be due to analytical uncertainties. Tetravalent cations Ti^{4+}, Hf^{4+}, Zr^{4+}, Th^{4+}, and U^{4+} do not follow simple parabolic patterns, possibly due to their complex site occupancies. Given its very small ionic radius, Ti likely occupies the small T site in plagioclase. As suggested by de Vries et al. (2012), Zr, Hf and Th partition coefficients may fall on the same parabola in the Onuma diagram, excluding U that may be present in part as U^{6+}. This hypothetical parabola (dashed lines in Fig. 4) renders an ideal lattice size (r_0) of 4+ cations on the M site (~0.95 Å) about 0.2–0.3 Å smaller than those of 1+, 2+, and 3+ cations (1.18–1.28 Å).

To obtain the lattice strain parameters for monovalent (Li^+, Na^+, and K^+), divalent (Ca^{2+}, Sr^{2+}, Ba^{2+}, Mg^{2+}),

Table 2
Lattice strain parameters derived from experimental partition coefficients.

Run #	An-Red-2	An-MORB-2
M^{1+}: Na^+, K^+, Li^+		
D_0	1.385	1.128
r_0 (Å)	1.208	1.232
E (GPa)	63	59
M^{2+}: Ca^{2+}, Mg^{2+}, Sr^{2+}, Ba^{2+}		
D_0	2.02(71)[a]	1.71(13)
r_0 (Å)	1.197(12)	1.199(3)
E (GPa)	164(23)	124(5)
M^{3+}: REE^{3+}, Y^{3+}		
D_0	0.057(3)	0.14(17)
r_0 (Å)	1.176(10)	1.28(10)
E (GPa)	187(16)	82(40)

[a] Numbers in parentheses are standard errors (1σ); 2.02(71) should be read as 2.02 ± 0.71. The standard errors cannot be obtained for monovalent cations due to zero degree of freedom.

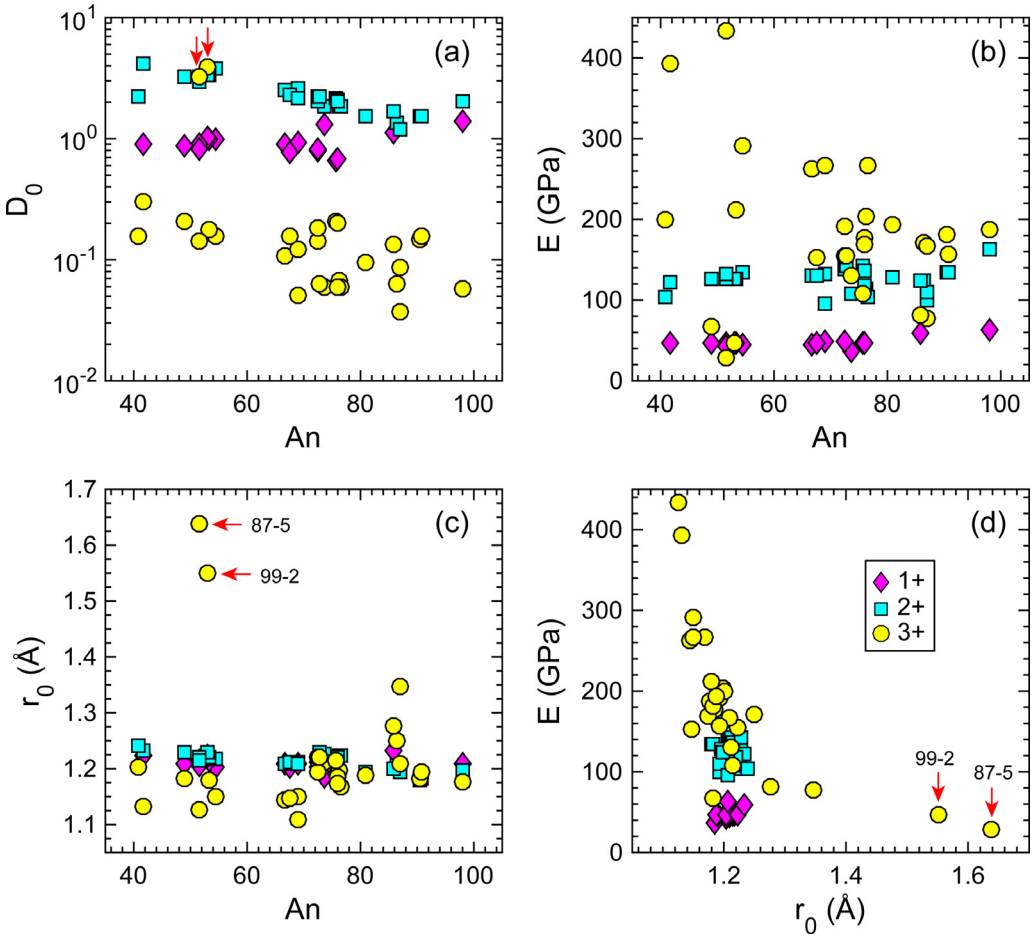

Fig. 5. Plots of best-estimated lattice strain parameters (D_0, E, and r_0) as a function of anorthite content (An) in plagioclase (a, b, c), and apparent correlation between E and r_0 due to the nonlinear nature the lattice strain model (d). The markers pointed by the red arrows are for run 99-2 from Bindeman and Davis (2000) and run 87-5 from Bindeman et al. (1998).

and larger trivalent cations (REE^{3+} and Y^{3+}), we apply the non-linear least squares method of Seber and Wild (1989) and fit the partition coefficients of each group to Eq. (2) by minimizing the Chi-square as defined below

$$\chi^2 = \sum_{i=1}^{N} (\ln D_i - \ln D_i^m)^2, \quad (4)$$

where D_i is defined by Eq. (2), D_i^m is the measured plagioclase-melt partition coefficient for element i, and N is the number of measured partitioning data used in the fit. We use logarithmic partition coefficients in our Chi-square calculation because the absolute concentrations of trace elements vary over orders of magnitude and because their abundances and partition coefficients are usually examined in semi-log spider diagrams. Similar to previous studies (e.g., Blundy and Wood, 1994), we use VIII-fold coordinated ionic radii for cations in the M site. The lattice strain parameters obtained in this study are listed in Table 2, and the best-fit curves are shown in Fig. 4.

Together with those inverted from published experiments, D_0 of REE and divalent cations decrease with the increase of plagioclase An, but those of monovalent cations appear to have a weak positive correlation with plagioclase An (Fig. 5a–c); r_0 of divalent cations display a negative correlation with An, while those of REE and monovalent cations do not show obvious correlations with An. The inverted r_0 and E for REE show a robust inverse correlation (Fig. 5d), indicating the strong trade-off between r_0 and E due to the nonlinear nature of the lattice strain model (Sun and Liang, 2012). This trade-off between r_0 and E may introduce significant uncertainties in the inverted lattice strain parameters, such as the abnormally high D_0 (>3) and r_0 (>1.5 Å) but small E (<50 GPa) for REE partitioning data from run 99-2 in Bindeman and Davis (2000) and from run 87-5 from Bindeman et al. (1998) (circles marked by red arrows in Fig. 5). In addition, low concentrations of heavy REE in plagioclase may induce large analytical uncertainties and thus result in considerable errors in the apparent lattice strain parameters. Because the numbers of elements are limited for monovalent and divalent cations, degrees of freedom are low and hence significant uncertainties may also be incorporated when inverting the lattice strain parameters. As demonstrated in recent studies on other mineral-melt systems (Sun and Liang, 2012, 2013a, 2013b; Yao et al., 2012; Dygert et al., 2014), a simultaneous

fit of selected experimental partitioning data to the lattice strain model can significantly increase the degree of freedom, and enables us to elucidate the effects of temperature, pressure and composition on trace element partitioning in plagioclase.

4. DEVELOPING NEW PARTITIONING MODELS

4.1. Data Compilation

In addition to our new experimental partitioning data, we also compiled plagioclase-melt trace element partition coefficients from published experimental studies with mineral and melt composition reported. The initial dataset contains 104 partitioning experiments from 12 studies (see Supplementary Figs. S2 and S3 for individual experiments. The experiments from Drake and Weill (1975) were not considered, because they were re-analyzed using SIMS by Bindeman et al. (1998) and Bindeman and Davis (2000). Surprisingly, many experiments from the literature show anomalous partition coefficients for REE in the Onuma diagram. This indicates the challenges of plagioclase-melt trace element partitioning studies, perhaps due to analytical issues and/or chemical disequilibrium. The compiled partitioning experiments were mostly conducted using slow cooling rates ($\leq$1 °C/min) or under isothermal conditions; however, 11 experiments in Dohmen and Blundy (2014) were conducted using faster cooling rates (2, 5.5 and 50 °C/min), which may result in growth rate-dependent partition coefficients (e.g., Mollo et al., 2011).

To ensure a self-consistent calibration dataset with minimal kinetic and analytical artifacts, we excluded partitioning experiments that meet any of the following criteria: (a) significant REE anomalies in the Onuma diagram (16 experiments; e.g., Run36 in Aigner-Torres et al., 2007), (b) no REE (13 experiments) or less than three REE data reported (8 experiments), (c) notably large analytical errors for REE (21 experiments; e.g., $1\sigma > 40\%$ on average in Laubier et al., 2014), and (d) fast cooling rates (11 experiments; e.g., cooling rates $\geq$2 °C/min in Dohmen and Blundy, 2014). The conservative approach in data screening yields 33 experiments from the literature, including 6 slow-cooling runs (0.02–0.05 °C/min) from Dohmen and Blundy (2014). However, significant heterogeneities in plagioclase compositions still appeared in some of the slow cooling runs from the latter study (e.g., Run 93-10a: 0.02 °C/min and An = 47–57 in plagioclase; no REE reported), indicating chemical disequilibrium. Therefore, in our initial attempt at model calibrations we will not include the experiments from Dohmen and Blundy (2014). However, the experimental data of Dohmen and Blundy (2014) and Laubier et al. (2014) are discussed in more detail in the online Supplementary Materials.

The selected experiments include 27 runs from 6 partitioning studies (Blundy et al., 1998; Bindeman et al., 1998; Bindeman and Davis, 2000; Aigner-Torres et al., 2007; Fabbrizio et al., 2009; Tepley et al., 2010) and two runs from the present study. The 29 experiments were conducted at 1127–1410 °C and pressures of 1 atm

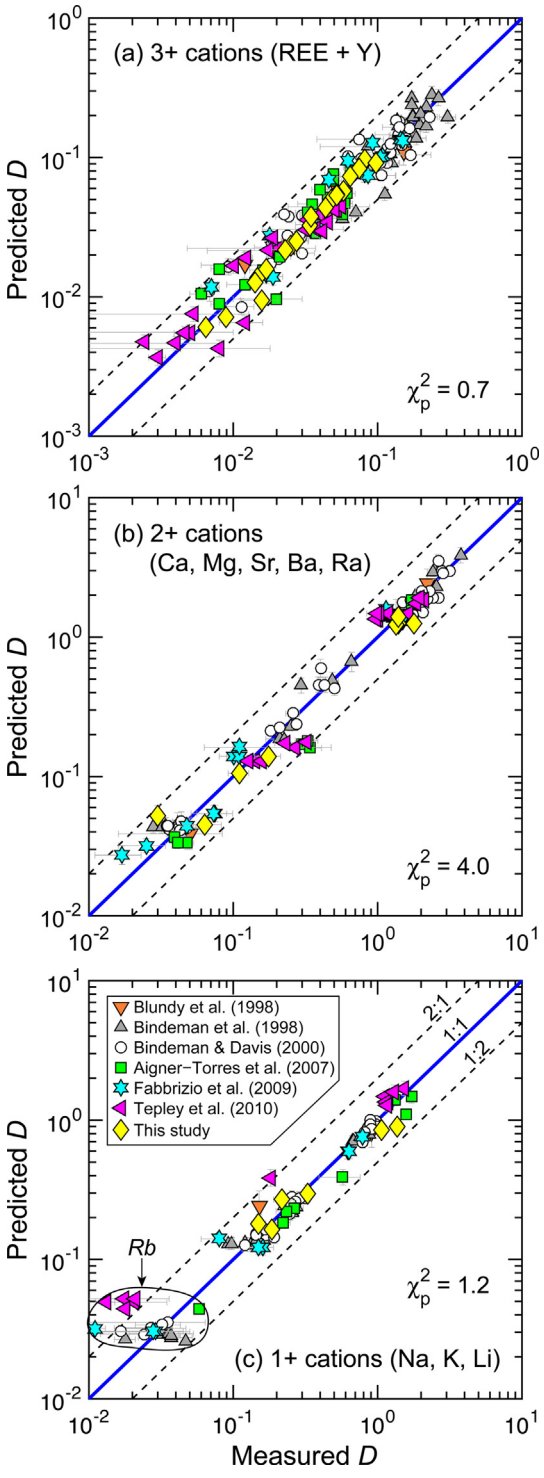

Fig. 6. Comparison between experimentally determined partition coefficients and model predicted values using Eqs. ((3), (6a)–(6c), (7a)–(7c), and (8a)–(8c)). Error bars represent standard deviation (1σ) of the measured partitioning data and 95% confidence interval (2σ) of the predicted values. The experimental partitioning data are the same as those displayed in Fig. 1. Given the large analytical errors, Rb partition coefficients were excluded from the model calibration but agree well with the model predicted values. See Supplementary Fig. S2 for individual experiments.

(26 literature experiments), 0.6 GPa (2 experiments in the present study), and 1.5 GPa (1 experiment from Blundy et al., 1998) under nominally anhydrous or water-saturated conditions (Fabbrizio et al., 2009). Plagioclase crystals and melts from these experiments cover a large range of composition (e.g., An = 41–98 in plagioclase; SiO_2 = 41.82–62.50 wt% and Mg# = 49–100 in melt).

Because Rb partition coefficients generally have large analytical errors, they were not used to calibrate the partitioning model but are shown in Fig. 6c. Misfits or outliers with reference to the lattice strain model (e.g., Eu anomaly) for individual experiments were also excluded in model calibrations. The final dataset contains 163 REE + Y partitioning data, 112 divalent element partitioning data (Ca, Mg, Sr, Ba, and Ra), and 70 monovalent element partitioning data (Na, Li, and K). Interested readers are referred to Supplementary Fig. S2 for Onuma diagrams for individual experiments. The REE partition coefficients vary by approximately one order of magnitude (e.g., D_{La} = 0.032–0.263, D_{Er} = 0.002–0.021), while those of divalent or monovalent cations vary by up to a factor of six (e.g., D_{Li} = 0.151–0.575, D_{Ba} = 0.100–0.661).

4.2. Parameterization methods

We have recently developed a protocol for analyzing trace element partitioning data using the lattice strain model and successfully applied it to REE + Y partitioning between major rock-forming minerals (clinopyroxene, orthopyroxene, olivine, garnet, and amphibole) and basaltic melts (Sun and Liang, 2012, 2013a, 2013b; Yao et al., 2012; Dygert et al., 2014; Shimizu, 2016). Here we expand the procedure described in Sun and Liang (2012) and develop parameterized lattice strain models for the partitioning of 1+, 2+ and 3+ cations through the following steps: (1) linear least squares analysis to identify key variables for each of the lattice strain parameters inverted from individual experiments, (2) simultaneous inversion of all filtered experimental data to constrain coefficients of the primary variables identified in step (1), and (3) joint inversion of partitioning data for 1+ and 2+ cations to further improve the goodness of the fit. The last step is necessary and unique for plagioclase as Ca, Na, and K are major elements in plagioclase and subject to stoichiometric constraints.

We assume that D_0 has the form of Eq. (2) in Sun and Liang (2012) and that r_0 and E are functions of plagioclase composition. Because of the nonlinear nature of the lattice strain model, we also allow E to vary as a function of r_0. Water abundances were not analyzed for the experimental melts, so no attempt was made to explore the water effect. After an extensive search of various permutations of the composition variables, we found that temperature and anorthite content (Ca or Na abundance) in plagioclase are the primary factors determining D_0, r_0 and E for 1+, 2+ and 3+ cations, which is consistent with earlier studies (e.g., Blundy and Wood, 1991; Bindeman et al., 1998; Bindeman and Davis, 2000; Aigner-Torres et al., 2007; Fabbrizio et al., 2009; Tepley et al., 2010; de Vries et al., 2012). In addition, we found that a pressure term is necessary to improve the fits to high-pressure partitioning data and that including the Na content in plagioclase results in a better fit for the divalent element partitioning data. Different from the log-linear formulation (Eq. (1)) used in the previous models, we found that D_0 and hence partition coefficients of REE + Y can be better reproduced through a quadratic relationship in log-scale with Ca content in plagioclase. Because a similar quadratic relationship provides fits for the partition coefficients of 1 + and 2+ cations as good as the log-linear formulation (Eq. (1)), here we use the same quadratic relationship between ln(D_0) and Ca in plagioclase for monovalent elements and that between ln (D_0) and Na in plagioclase for divalent elements.

For REE, D_0 is negatively correlated with Ca abundance in plagioclase and pressure but positively correlated with temperature, and r_0 and E can be treated as constants. For the divalent cations (Ca, Mg, Sr, Ba, and Ra), D_0 is negatively correlated with temperature and pressure but positively correlated with Na abundance in plagioclase, r_0 displays a positive correlation with Na abundance in plagioclase, and E can be treated as a linear function of r_0. For the monovalent cations (Na, K, and Li), D_0 is positively correlated with Ca abundance in plagioclase and pressure but negatively correlated with temperature, and r_0 and E can be treated as constants.

To further quantify the relationships identified above, we used the coefficients from the multiple linear regressions as initial inputs and carried out the global or simultaneous inversion to constrain the coefficients in the parameterized lattice strain model by minimizing the Chi-squares as defined in Eq. (4) for individual groups of isovalent cations, respectively. Note that N in Eq. (4) becomes the total number of measured partitioning data for individual groups of isovalent cations from the compiled dataset (i.e., N = 163 for REE + Y, 112 for divalent cations, and 70 for monovalent cations). To better assess the goodness of fit and to compare with previous models, we calculated the Pearson's Chi-square (χ^2_p) after the inversion using Eq. (2).

Because the estimated Ca, Na, and K partition coefficients have to satisfy the constraints of measured anorthite and albite contents in plagioclase, we performed a final joint inversion to fit all partitioning data of monovalent and divalent elements (N = 182) together with plagioclase An and Ab (=100 × Na/(Ca + Na + K) in mole) by minimizing the Chi-square

$$\chi^2_{\text{joint}} = \sum_{j=1}^{N=182} (\ln D_j - \ln D_j^m)^2 + \sum_{i=1}^{N=29} \left[(\ln X_i - \ln X_i^m)^2 + (\ln Y_i - \ln Y_i^m)^2 \right], \quad (5)$$

where X_i^m and Y_i^m are the measured An and Ab, respectively, in plagioclase from experiment i; and X_i and Y_i are the model predicted An and Ab. The joint inversion further improves the models constrained by independent inversions of monovalent and divalent element partitioning data in Step 2 as shown by the reduction of Pearson's Chi-squares (See Section S5 in the online Supplementary Materials). Given the additional constraints of An and Ab,

results of the joint inversion are preferred for the monovalent and divalent element partitioning.

4.3. Model results

Through a global fit to all trivalent element (REE + Y) partitioning data ($N = 163$) from the 29 selected experiments, we obtained the following expressions for the lattice strain parameters that control the REE + Y partitioning between plagioclase and silicate melt:

$$\ln D_0^{3+} = 16.05(\pm 1.57) - \frac{19.45(\pm 1.78) + 1.17(\pm 0.14)P^2}{RT} \times 10^4 - 5.17(\pm 0.37)(X_{Ca})^2, \quad (6a)$$

$$r_0^{3+}\ (\text{Å}) = 1.179(\pm 0.027), \quad (6b)$$

$$E^{3+}\ (\text{GPa}) = 196(\pm 51), \quad (6c)$$

where X_{Ca} is the Ca content in plagioclase per eight-oxygen; P is pressure in GPa; and numbers in parentheses are 2σ uncertainties estimated directly from the simultaneous inversion.

The joint global inversion of all monovalent and divalent element partitioning data ($N = 182$) as well as An and Ab in plagioclase result in the following lattice strain parameters for the divalent elements:

$$\ln D_0^{2+} = \frac{6910(\pm 985) - 2542(\pm 1372)P^2}{RT} + 2.39(\pm 0.52)(X_{Na})^2, \quad (7a)$$

$$r_0^{2+}\ (\text{Å}) = 1.189(\pm 0.005) + 0.075(\pm 0.016)X_{Na}, \quad (7b)$$

$$E^{2+}\ (\text{GPa}) = 719(\pm 309) - 487(\pm 255)r_0^{2+}, \quad (7c)$$

where X_{Na} is the Na content in plagioclase per eight-oxygen and is equivalent to $(1 - X_{Ca} - X_K)$ in plagioclase with balanced stoichiometry. The coefficients of the temperature and pressure terms in Eq. (7a) are about 3–5 times smaller than those in Eq. (6a), indicating that divalent element partitioning in plagioclase is not strongly affected by temperature or pressure.

Lattice strain parameters for the monovalent cations derived from the joint global inversion also include a pressure term to better fit the high-pressure partitioning data from the two experiments (0.6 GPa) reported in this study and the one (1.5 GPa) from Blundy et al. (1998):

$$\ln D_0^{1+} = -9.99(\pm 1.76) + \frac{11.37(\pm 1.95) + 0.49(\pm 0.23)P}{RT} \times 10^4 + 1.70(\pm 0.38)(X_{Ca})^2, \quad (8a)$$

$$r_0^{1+}\ (\text{Å}) = 1.213(\pm 0.007), \quad (8b)$$

$$E^{1+}\ (\text{GPa}) = 47(\pm 3). \quad (8c)$$

Replacing the lattice strain parameters in Eq. (3) by Eqs. (6a)–(6c), (7a)–(7c), and (8a)–(8c), we obtained generalized lattice strain models for the partitioning of 3+, 2+, and 1+ cations between plagioclase and silicate melt, respectively. In the online Supplementary Materials, a simple Excel program is presented to calculate plagioclase-melt trace element partition coefficients for a plagioclase composition at given temperature and pressure. Fig. 6 shows that the partition coefficients predicted by our new models are in excellent agreement with those determined experimentally (see Supplementary Fig. S2 for model predicted partition coefficients of individual experiments). The χ_p^2 values derived from our models are approximately 1.5–15 times smaller than those calculated using the previous models (Fig. 1 and Supplementary Fig. S1), indicating the significant improvement of our new models. Although Rb and Cs partition coefficients were not used for model calibrations, our model for monovalent element partitioning predicts their partition coefficients well within the margin of analytical errors (Fig. 6c and Supplementary Fig. S2). The anomalous REE partition coefficients from the excluded experiments significantly deviated from our model predicted values (Supplementary Figs. S3 and S4). Interestingly, our model predicted partition coefficients for 1+ (Na, K, Li) and 2+ cations (Mg, Ca, Sr, Ba) agree very well with the measured values from most of the excluded experiments. This indicates that 1+ and 2+ element partitioning data likely remain valid in most of the excluded experiments (Supplementary Fig. S5), perhaps due to the faster diffusion of 1+ and 2+ cations in plagioclase (e.g., Cherniak, 2010; and references therein).

Consistent with our earlier studies on REE partitioning in pyroxenes, garnet, and olivine and HFSE partitioning in low-Ca pyroxene (Sun and Liang, 2012, 2013a, 2013b; Yao et al., 2012), these new models for the partitioning of 1+, 2+, and 3+ cations between plagioclase and silicate melt also indicate that temperature and mineral composition are the dominant factors controlling trace element partitioning in plagioclase. As a controlling factor for plagioclase saturation in silicate melt (e.g., Putirka, 2005; Lange et al., 2009; Namur et al., 2012), melt composition also influences trace element partitioning in plagioclase through plagioclase-melt phase equilibria (e.g., Dohmen and Blundy, 2014). In the parameterized model of Namur et al. (2012), for example, An content in plagioclase depends on temperature and coexisting melt composition (see their Eqs. (31) and (33)).

4.4. Sources of uncertainties and model limitations

The new lattice strain models presented in this study can recover the selected experimental partitioning data to within 20% standard deviation on average. However, small discrepancies still appear between the model predicted partition coefficients and the experimentally determined ones in Fig. 6. The sources of discrepancies include analytical errors, chemical disequilibrium in the experiments, biases of the partitioning experiments among different laboratories, and limitations of our models. Given their low abundances in plagioclase, highly incompatible elements (e.g., heavy REE) are more challenging to determine analytically, and thus may induce errors in the models. Because Ca is a major element in plagioclase, errors on the predicted Ca partition coefficients are attributed to its non-Henrian behavior. Although we set conservative criteria to exclude

experiments with possible kinetic effects, small extents of disequilibrium may still exist in the selected experiments. Among the 29 selected experiments there are only three high-pressure runs (2 runs at 0.6 GPa from this study and one at 1.5 GPa from Blundy et al. (1998)), and none of the 29 experiments cover Fe-rich and silicic systems, or low-An plagioclase (An < 40). Thus, care should be taken when applying our models to the aforementioned conditions, which demand more partitioning studies from laboratory experiments or field validation.

4.5. Model tests

Three recent studies measured plagioclase-melt partition coefficients through LA-ICP-MS analyses of trace element abundances in plagioclase phenocrysts and their equilibrium melt phases (melt inclusion or glass matrix) from three different volcanic lavas (e.g., Zajacz and Halter, 2007; Severs et al., 2009; Fedele et al., 2015). These field-based partitioning data cover a broader range of temperature (1000–1228 °C) and composition (An = 29–82; SiO_2 = 53–66 wt%, Mg# = 19–52, and H_2O = ~0.6–4 wt% in melt) and allow us to assess the validity of our partitioning models for Fe-rich and silicic systems, low-An (<42) plagioclase, and low temperatures (<1142 °C).

Zajacz and Halter (2007) analyzed plagioclase phenocrysts (An = 82) and melt inclusions (SiO_2 = 53 wt% and Mg# = 52) from a late-Holocene basaltic-andesite at Villarrica, Chile. Although water abundance was not determined for melt inclusions, the bulk rock (SiO_2 = 57 wt% and Mg# = 52) has a total of 98.2 wt% major oxides, indicating possible presence of water in the melt inclusion. Severs et al. (2009) reported compositions of plagioclase phenocrysts (An = 66) and melt inclusions (SiO_2 = 66 wt % and Mg# = 38) in a dacite from the 1988 eruption at White Island, New Zealand. Ion probe analyses indicate 0.6 ± 0.2 wt% H_2O in plagioclase-hosted melt inclusions from the 1989 eruption (Wardell et al., 2001). Similar amounts of water are also likely present in the melt inclusions from the 1988 eruption. Fedele et al. (2015) investigated quenched trachytic and trachyphonolitic glass matrices (SiO_2 = 60–62 wt%, Mg# = 16–21, and Na_2O = 5–6 wt%) and coexisting plagioclase phenocrysts (An = 27–30) from three samples. Because the three samples are nearly identical in plagioclase and melt compositions, here we treated them as one sample by averaging the plagioclase and melt compositions, respectively. As demonstrated through FTIR analyses of melt inclusions from the same eruption (Marianelli et al., 2006), these trachyphonolitic lavas initially have 4 ± 1 wt% H_2O during phenocryst crystallization.

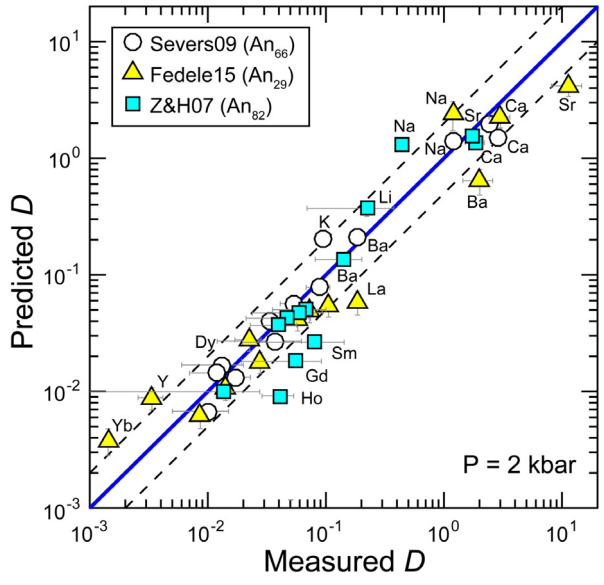

Fig. 7. Comparison between field-measured partition coefficients and model predicted values calculated using Eqs. ((3), (6a)–(6c), (7a)–(7c), and (8a)–(8c)) for plagioclase phenocrysts and their equilibrium melts (melt inclusions or quenched glasses) reported in Zajacz and Halter (2007), Severs et al. (2009), and Fedele et al. (2015). The compositions of plagioclase and melt were determined by electron microprobes for major elements and by LA-ICP-MS for trace elements. The equilibrium temperatures were calculated at 2 kbar using the plagioclase saturation thermometer of Putirka (2005). See text for details of these samples.

With these estimated H_2O abundances in the melt, we calculated the plagioclase-melt equilibrium temperatures by applying the widely used plagioclase saturation thermometer of Putirka (2005) to the aforementioned samples. Assuming a pressure of 2 kbar, we obtained temperatures 1216 °C, 1154 °C, and 1000 °C for samples from Villarrica, White Island, and Campi Flegrei, respectively. Assuming equilibrium partitioning of trace elements between the plagioclase and coexisting melt, we can use the measured plagioclase major element compositions, the estimated temperatures, and our parameterized lattice strain models (Eqs. (3), (6a)–(6c), (7a)–(7c), and (8a)–(8c)) to calculate plagioclase-melt partition coefficients for Ca, Ba, Sr, Na, K, Li, Y, and REE. Fig. 7 shows that the partition coefficients derived from our models are in good agreement with the field-measured values. Despite their low abundances in plagioclase and hence large analytical errors, most REE still fall on the one-to-one correlation line, indicating that our model for REE partitioning in plagioclase may be extrapolated to lower temperatures and more evolved compositions (Fe-rich and silicic). However, our model for monovalent element partitioning overestimates Na partition coefficients for the two hydrous samples (Zajacz and Halter, 2007; Fedele et al., 2015) by about a factor of two. The overestimates of Na partition coefficients may be due to analytical uncertainties or perhaps effects of water on melt structure and plagioclase-melt phase equilibria.

4.6. Physical meanings of the lattice strain parameters

4.6.1. Strain-free partition coefficients D_0

For a group of isovalent cations partitioning into the same lattice site, D_0 follows the generic thermodynamic equation (e.g., Wood and Blundy, 1997; van Westrenen et al., 2001; van Westrenen and Draper, 2007)

$$\ln D_0 = \frac{\Delta H}{RT} - \frac{\Delta S}{R} + \frac{P\Delta V}{RT} + (\ln \gamma^{melt} - \ln \gamma^{min}), \quad (9)$$

where ΔS, ΔH and ΔV are the changes of entropy, enthalpy and volume of the exchange of an ideal cation between the crystal and melt; γ^{min} and γ^{melt} are the activity coefficients of the cation (or its component) in the crystal and melt, respectively. As demonstrated in our previous models for REE and HFSE partitioning between mantle minerals (olivine, pyroxenes, and garnet) and basaltic melts (Sun and Liang, 2012, 2013a, 2013b; Yao et al., 2012; Dygert et al., 2014), the effect of melt composition appears to be indirect through mineral saturation in silicate melt. Interestingly, for all three groups of cations in the plagioclase M site, D_0 share the same compositional term, $(X_{Ca})^2$, or its equivalent, $(X_{Na})^2$, which mimics $\ln \gamma^{min}$ in Eq. (9) and indicates that a simple regular solution model (i.e., one-parameter Margules activity model) may be applicable to mixing of anorthite (or albite) and plagioclase components of ideal 1+, 2+, and 3+ cations. The compositional terms in our models are also consistent with the activity model of Holland and Powell (1992) derived from Darken's quadratic formalism, and confirm the importance of anorthite content on trace element partitioning in plagioclase as demonstrated in previous studies (e.g., Blundy and Wood, 1991; Bindeman et al., 1998; Bindeman and Davis, 2000; Bédard, 2006; Tepley et al., 2010; Hui et al., 2011).

The temperature terms in D_0 are related to ΔH of the ideal cation exchange between plagioclase and melt. The coefficient of the temperature term in D_0 of monovalent cations (Eq. (8a)) corresponds to $\Delta H = 114 \pm 20$ kJ/mol, which is comparable to the heat of fusion of albite (64.5 kJ/mol; e.g., Stebbins et al., 1982; Tenner et al., 2007) and anorthite (135 kJ/mol; Weill et al., 1980), whereas those in D_0 of divalent and REE cations indicate significantly smaller ΔH (7 ± 1 kJ/mol for 2+ cations, and -194 ± 18 kJ/mol for 3+ cations) than the plagioclase heat of fusion. Notably, the coefficient of the temperature term in D_0 of trivalent cations is negative with an absolute value considerably larger than that of monovalent and divalent cations. As D_0 determines the peak value of the parabola in the Onuma diagram (Fig. 4), the coefficient of the temperature terms in Eqs. (6a), (7a) and (8a) indicate that temperature has the most significant effect on REE partitioning but small to negligible influence on the partitioning of monovalent and divalent cations. The weak temperature dependence of divalent cation partitioning has also been suggested in the study of Blundy and Wood (1991) based on Sr and Ba partitioning in plagioclase.

The pressure terms in D_0 correspond to $P\Delta V$ of the ideal cation exchange between plagioclase and melt. The coefficient of the pressure term in Eq. (8a) indicates a constant volume change for the ideal 1+ cation exchange between plagioclase and melt; however, the second-order pressure terms in Eqs. (6a) and (7a) suggest pressure-dependent volume changes for the ideal 2+ and 3+ cation exchange. Because the coefficients of the pressure terms for all three groups of cations are significantly smaller than those of the temperature terms and because the plagioclase stability is restricted to low pressures, the pressure effect on element partitioning in plagioclase is overwhelmed by the temperature effect.

4.6.2. Effective Young's modulus E and ideal lattice size r_0

Previous studies suggest that E generally varies with cation charge, lattice site, temperature, pressure, and crystal chemistry while r_0 depends on crystal structure and may change with crystal chemistry (e.g., Blundy and Wood, 1994; Gaetani and Grove, 1995; Wood and Blundy, 1997; Lundstrom et al., 1998; van Westrenen et al., 1999, 2001; van Westrenen and Draper, 2007; Hill et al., 2000, 2011; Frei et al., 2009; Sun and Liang, 2012, 2013a, 2013b; Yao et al., 2012; Dygert et al., 2014). In plagioclase, E and r_0 of 1+ and 3+ cations on the M site do not appear to be composition dependent (Eqs. (6b)–(6c), (7c), and (8b)–(8c)), while those of 2 + cations vary as a linear function of albite content (Eqs. (7b)–(7c)).

Interestingly, E of 1+ cations (48 ± 3 GPa) is nearly identical to the bulk moduli of low albite (52.3 ± 0.9 GPa) from Benusa et al. (2005) and analbite (50.3 ± 0.5 GPa) from Curetti et al. (2011). E of 2+ cations from the compiled experiments (116–140 GPa) are much larger than the bulk modulus ($K = 80.4 \pm 0.7$ GPa; Angel, 2004) of high-An plagioclase (An_{89}), but can be related to the bulk modulus K through the following equation (Blundy and Wood, 1994),

$$E = 3K(1 - 2\upsilon), \tag{10}$$

where υ is the Poisson's ratio of the material and was assumed as 0.25 for all minerals. As no REE end-members of plagioclase exist, E of 3+ cations cannot be compared with the corresponding K. For all three groups of cations in plagioclase, E is positively correlated with the cation charge, which agrees well with the Hazen–Finger relationship (Hazen and Finger, 1979) derived for homogeneous isotropic materials (Fig. 8a). A small discrepancy appears between E of 1+ cations and the Hazen-Finger relationship. This may be due to the empirical relationship between E and K (Eq. (10)) or drawbacks of the Hazen-Finger relationship.

Similar to those observed in Wood and Blundy (2003), r_0 of 2+ cations display a weak negative correlation with Ca content in plagioclase. The An range (= 41–98) of the selected experimental partitioning data only yields a rather small variation of r_0 (1.19–1.23 Å) for the divalent cations. Although it appears that r_0 decreases with the cation charge (Fig. 8b), r_0 of 1+ cations is just 0.03 Å greater than that of 3+ cations, consistent with the same site occupancy (M) of the 1+, 2+, and 3+ cations in plagioclase. The weak dependence of r_0 upon plagioclase composition and cation charge can be attributed to the small difference in ionic radii between Ca^{2+} and Na^{+} (1.12 Å vs. 1.18 Å; VIII-fold coordination; Shannon, 1976). As E and r_0 of 3+ cations have large error bars, they may also weakly depend on plagioclase chemistry, which cannot be resolved based on the available experimental data.

5. APPLICATIONS

5.1. Partitioning of Ra/Ba and Implication for Ra-Th Dating

The disequilibrium between short-lived ^{226}Ra and its parent ^{230}Th has been widely used to estimate

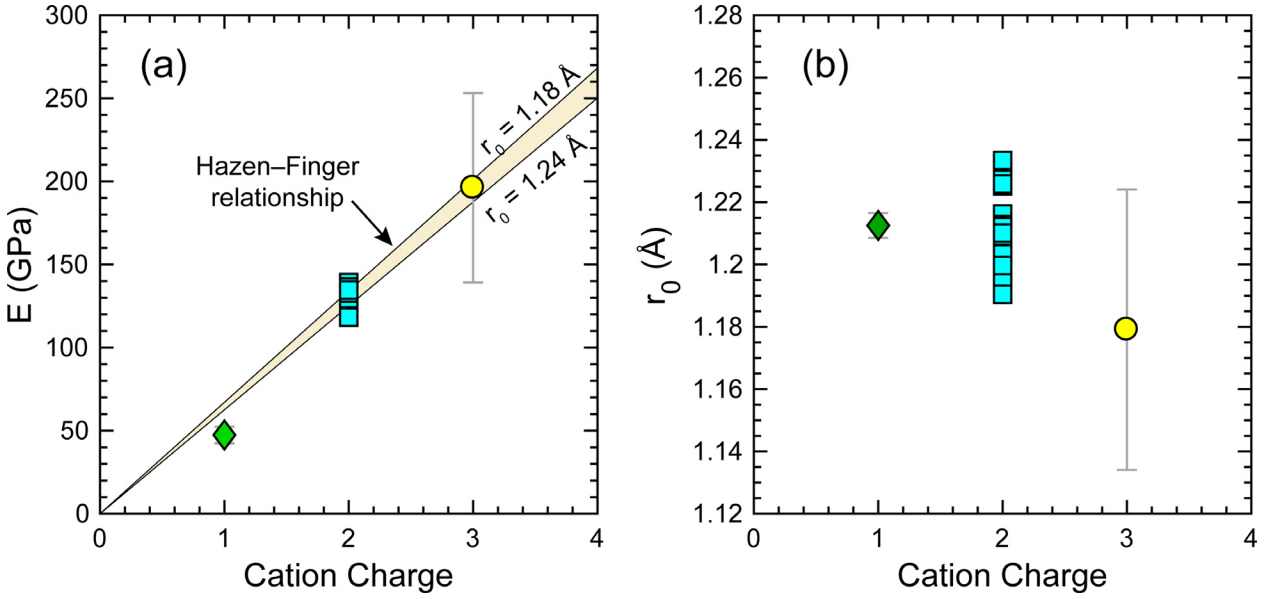

Fig. 8. Variations of the apparent Young's Moduli (E); (a) and ideal lattice size (r_0); (b) for monovalent, divalent, and trivalent elements on the M site as a function of the cation charge. E and r_0 are from Eqs. (6b)–(6c), (7b)–(7c), and (8b)–(8c). Error bars indicate 2σ errors. Since E and r_0 for divalent elements are a function of Na content in plagioclase, a range of E and r_0 were calculated for the compiled experiments using Eqs. (7b) and (7c). The Hazen–Finger relationship was calculated using Eq. (4) in Wood and Blundy (2003) for a range of r_0 (1.18–1.24 Å).

crystallization ages of phenocrysts in pre-eruption volcanic lavas (e.g., Volpe and Hammond, 1991; Cooper et al., 2001; Cooper and Reid, 2003; Tepley et al., 2006; Zellmer et al., 2008). Without the existence of a stable Ra isotope, Ba is often taken as a proxy to track Ra fractionation during magma crystallization, assuming that Ra and Ba have similar compatibilities. Thus, the Ra-Th dating on plagioclase requires quantitative understanding of the relative partitioning behaviors of Ra and Ba in plagioclase.

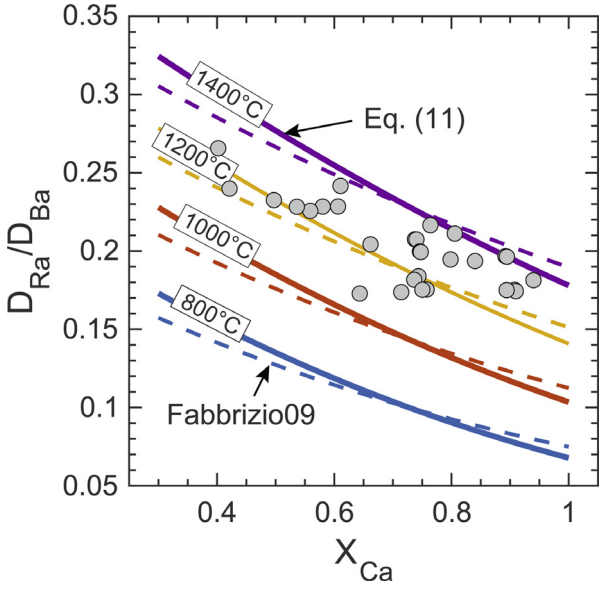

Fig. 9. Calculated ratios of Ra and Ba partition coefficients as a function of Ca content in plagioclase per eight-oxygen (X_{Ca}) at four selected temperatures. Solid curves were derived from Eq. (11), while dashed curves were calculated using the model of Fabbrizio et al. (2009). Gray markers denote values derived using Eq. (11) for the compiled experiments.

Using the constant lattice strain parameters (E and r_0) reported in Blundy and Wood (1994), Cooper et al. (2001) calculated plagioclase-melt Ra and Ba partition coefficients for two selected temperatures (1100 °C and 1160 °C) and plagioclase compositions (An = 60 and 70). They obtained a very small variation of D_{Ra}/D_{Ba} (0.21–0.25) for the four considered cases, which is similar to that from a recent experimental study on anorthite-melt Ra partitioning ($D_{Ra}/D_{Ba} = 0.24 \pm 0.07$; Miller et al., 2007). Recently, Fabbrizio et al. (2009) suggested that the relative partitioning behaviors of Ra and Ba (D_{Ra}/D_{Ba}) strongly depend on An in plagioclase and temperature. By fitting the partitioning data from four of their experiments (An = 34, 81, 91, and 91) and the one in Miller et al. (2007; An = 100), they proposed log-linear formulations (cf. Eq. (1)) for plagioclase-melt Ra and Ba partitioning. Applying their models to literature data, they argued that D_{Ra}/D_{Ba} of many plagioclase phenocrysts are systematically smaller than the suggested values (0.21–0.25) by Cooper et al. (2001) and therefore the literature Ra-Th ages are overestimated by ~20–90% in previous studies.

The new model presented in this study enables us to further assess Ba and Ra partitioning in plagioclase. Using the lattice strain parameters (E and r_0) calibrated in this study for divalent cations (Eqs. (7b)–(7c)), we have the following expression quantifying the relative partitioning of Ra and Ba in plagioclase,

$$\frac{D_{Ra}}{D_{Ba}} = \exp\left(-\frac{24,014 - 13,209X_{Na} + 1,812(X_{Na})^2}{RT}\right). \quad (11)$$

Fig. 9 displays values of D_{Ra}/D_{Ba} derived from Eq. (11) (solid curves) for a wide range of plagioclase composition ($X_{Ca} = 0.3–1.0$; equivalent to An = 30–100) at four representative temperatures (800 °C, 1000 °C, 1200 °C, 1400 °C). D_{Ra}/D_{Ba} are positively correlated with temperature but negatively correlated with Ca content in plagioclase. At a given temperature, a decrease of 70 mol% anorthite content in plagioclase results in a 0.12 decrease in D_{Ra}/D_{Ba}, which is similar to that derived from a 400 °C temperature increase for a fixed plagioclase composition. The predicted D_{Ra}/D_{Ba} for the compiled experiments (1127–1410 °C; An = 41–98) display a considerable variation (0.17–0.27; gray dots in Fig. 9). Hence, better estimations of D_{Ra}/D_{Ba} for Ra-Th dating can be obtained using Eq. (11) for specific plagioclase crystals at relevant temperatures.

The model of Fabbrizio et al. (2009) produces D_{Ra}/D_{Ba} (dashed curves in Fig. 9) similar to those (solid curves) derived from Eq. (11) for the same temperature and compositional spaces. However, small but systematic differences appear in the predicted D_{Ra}/D_{Ba} between our model and that of Fabbrizio et al. (2009). The values of D_{Ra}/D_{Ba} calculated using the model of Fabbrizio et al. (2009) appear to be smaller than those derived from Eq. (11) for low An plagioclase by up to 0.02. The systematic differences are likely due to uncertainties of linear regressions in Fabbrizio et al. (2009), in which the slopes were mainly constrained by one experiment (Run 31) with low An (= 34) (see their Fig. 4).

5.2. HFSE and noble gas partitioning

In plagioclase, D_0 of 1+, 2+, and 3+ cations on the M site display a near-parabolic relationship with the cation charge (Fig. 10a) and can be quantified by the electrostatic model of Wood and Blundy (2003),

$$D_0^{Z+} = D_{00} \exp\left[\frac{-\Phi}{RT}(Z - Z_0)^2\right], \quad (12)$$

where Φ is a factor for the electrostatic work; Z is the charge of the ideal cation; Z_0 is the charge of major cations in the lattice site; and D_{00} is the strain-free partition coefficients for cations of charge Z_0. According to the Hazen-Finger relationship (Fig. 8a), E of noble gases (0+) is zero, but those of 4+ and 5+ cations on the M site are significant (~250 GPa and ~300 GPa, respectively). Because of the trivial E, D_0 of noble gases (0+) are effectively their partition coefficients, whereas all three lattice-strain parameters (D_0, r_0, and E) are required to estimate the absolute values of 4+ cation partition coefficients on the M site.

The partition coefficients of tetravalent HFSE (Th, U, Zr, Hf and Ti) from our compiled experiments are all about 1–2 orders of magnitude greater than the D_0 of 4+ cations on the M site defined by the electrostatic model (Fig. 10a), while pentavalent HFSE partition coefficients (Nb, and Ta) are even larger (>3 orders of magnitude) than D_0 of 5+ cations on the M site. The significant differences are similar to the observation on D_U in Blundy and Wood (2003) and indicate that HFSE may not preferentially enter the same site (M) as the large 1+, 2+, and 3+ cations. Alternatively, the predicted D_0 of the 4+ and 5+ cations on the M site may not simply follow the electrostatic model. Future studies on the site occupancies and diffusion of 4+ cations are needed to better understand HFSE partitioning in plagioclase.

Experimental data on noble gas partitioning between plagioclase and melt are sparse. Broadhurst et al. (1990) reported the first experimental anorthite-melt Ar partition coefficient (0.6 ± 0.5) that is comparable to those for olivine and pyroxene from their experiments. As their partitioning data for noble gases are generally about 1–5 orders of magnitude greater than those for olivine and pyroxene from more recent experimental studies (on the order of 10^{-4}; e.g., Brooker et al., 2003; Heber et al., 2007; Jackson et al., 2013), their partitioning data have been questioned and believed to have melt or gas contaminations (see discussion in Brooker et al., 2003). On the contrary, the preliminary plagioclase-melt Ar partition coefficients (0.007–0.036) provided by Carroll et al. (1994) are about 1–2 orders of magnitude smaller than that from Broadhurst et al. (1990). Surprisingly, Carroll et al.'s Ar partition coefficients are compatible with the electrostatic model for heterovalent cation partitioning on the M site (Fig. 10a). This confirms that noble gases preferentially enter the M site in plagioclase and that their partition coefficients can be quantified through a generalized electrostatic model.

Given D_0 of 1+, 2+, and 3+ cations calculated using Eqs. (6a), (7a), and (8a) for individual experiments, we can eliminate the three unknown electrostatic parameters (Φ, Z_0, and D_{00}) and solve for noble gas partition coefficients (D_0 of 0+ cations) through the following expression

$$D_0^{0+} = (D_0^{1+})^3 (D_0^{3+})/(D_0^{2+})^3. \quad (13)$$

Combining Eq. (13) with the expressions for D_0 of 1+, 2+, and 3+ cations (Eqs. (6a), (7a), and (8a)), we obtain a model for noble gas partitioning between plagioclase and silicate melt,

$$\ln D_0^{0+} = -13.93 + \frac{12.58 + 1.47P - 0.41P^2}{RT} \times 10^4 - 0.06(X_{Ca})^2 - 7.17(X_{Na})^2. \quad (14)$$

This model indicates that noble gas partition coefficients are positively correlated with Ca content in plagioclase and pressure but are inversely correlated with temperature. A 50 mol% increase of anorthite content in plagioclase increases the noble gas partition coefficient by about one order of magnitude, which effectively is equivalent to a temperature decrease of ~200 °C (Fig. 10b). As pressure increases from 1 bar to 1 GPa, noble gas partition coefficients increase by about a factor of two, indicating a relatively small pressure effect.

The estimated plagioclase-melt noble gas partition coefficients (0.003–0.025) for our compiled experiments are comparable to the preliminary experimental data for Ar (0.007–0.036) from Carroll et al. (1994) and are about one to two orders of magnitude greater than those of olivine, pyroxene, and spinel in the literature (on the order of 10^{-4}; e.g., Brooker et al., 2003; Heber et al., 2007; Jackson et al., 2013). This is possibly due to the relatively open crystal structure of plagioclase. The relatively large noble gas partition coefficients in plagioclase indicate that

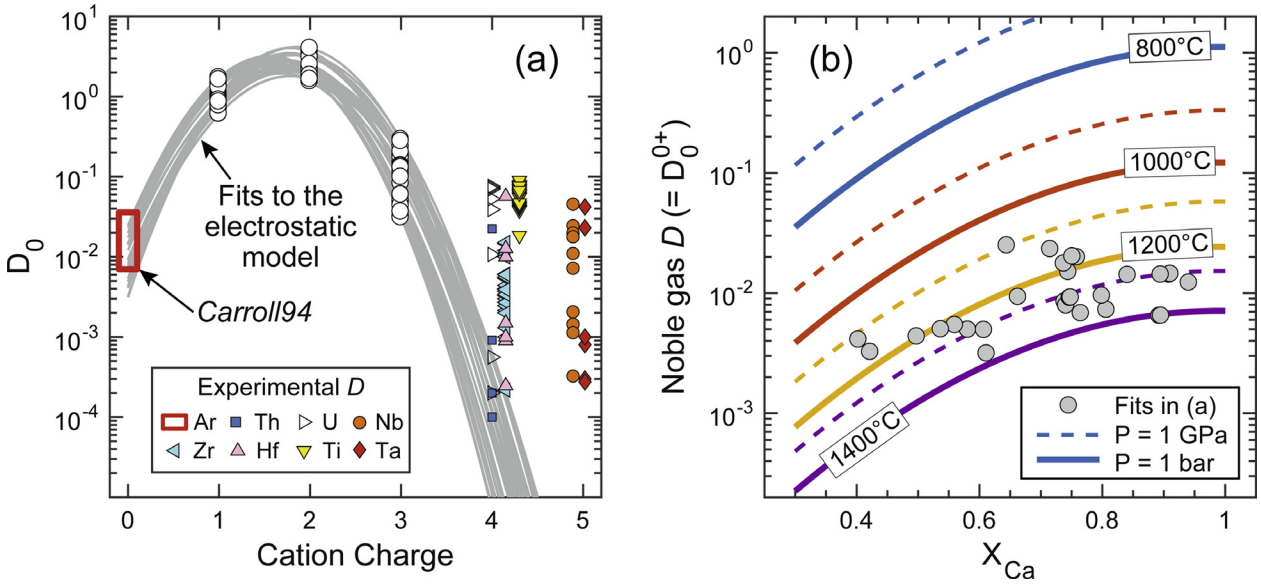

Fig. 10. Plots showing D_0 as a function of the cation charge (a) and the calculated noble gas partition coefficient as a function of Ca content in plagioclase at four selected temperatures and two choices of pressures (b). D_0 were calculated using Eqs. (6a), (7a), and (8a). Red rectangle in (a) denotes the range of plagioclase-melt Ar partition coefficients from the preliminary experiments of Carroll et al. (1994). Gray curves in (a) are the fits to the electrostatic model (Eq. (12)) for individual experiments, while the gray markers in (b) are the corresponding noble gas partition coefficients calculated from the electrostatic model (Eq. (14)). For better visibility, the experimental partitioning data for U, Zr, Hf, Ti, and Nb in (a) are slightly off their corresponding cation charges. (For interpretation of the references to color in this figure legend, the reader is referred to the web version of this article.)

plagioclase crystallization may significantly influence noble gas fractionation. Anorthite crystallization and floatation may have played a central role in noble gas budget of the Moon.

5.3. Partition coefficients for terrestrial and lunar magmatism

The new parameterized lattice strain models developed in this study allow us to assess the chemical fractionation of terrestrial and lunar magmas involving plagioclase. In this section, we consider variations of plagioclase-melt partition coefficients during fractional crystallization of MORB and the lunar magma ocean, respectively.

5.3.1. Mid-ocean ridge basalt crystallization

Differentiation of MORB was calculated using the MELTS program (Ghiorso et al., 2002; Smith and Asimow, 2005) for isobaric fractional crystallization of a primary MORB (Workman and Hart, 2005) under anhydrous conditions with fO_2 at two logarithmic units below the quartz–fayalite–magnetite buffer. To examine the pressure effect, we considered two end-member cases: 0.5 kbar and 5 kbar. In the former case, plagioclase becomes saturated in the melt at 1227 °C after 1% olivine crystallization; in the latter case, plagioclase starts to crystallize at a higher temperature, 1264 °C, after 12% fractionation of clinopyroxene and spinel. Because MELTS fails at low temperatures, we terminated the crystallization calculations at 1050 °C. As crystallization proceeds with decreasing temperature, plagioclase continues to solidify with decreasing anorthite content, while plagioclase crystals in the low-pressure (0.5 kbar) case have systematically higher anorthite content than those in the high-pressure (5 kbar) case at the same temperatures. Effectively, plagioclase An and temperatures display two parallel positive relationships for the two cases (see inset in Fig. 11a).

Applying the new parameterized models for plagioclase-melt trace element partitioning, we calculated partition coefficients for plagioclase crystallized from MORB at 0.5 kbar and 5 kbar. Fig. 11a displays the plagioclase-melt partition coefficients for the low-pressure case (0.5 kbar) at 1%, 40%, and 90% solidification, which cover their variability throughout the crystallization process. The predicted partition coefficients for the high-pressure case (5 kbar) are shown by the light blue region. Despite the large ranges of temperature and plagioclase An content during MORB crystallization, the calculated partition coefficients display small to moderate variations. For both cases, the partition coefficients of noble gases (Ar^*) and monovalent elements (Na, Li, K, Rb, Cs) are nearly constant, while those of REE increase within about a factor of two as temperature drops from the liquidus to ~1050 °C (>90% solidification).

Because REE partition coefficients are positively correlated with temperature but negatively correlated with Ca content in plagioclase, the apparent positive correlation between temperature and plagioclase An during MORB crystallization induces the competition between these two and further results in the small variations of REE partition coefficients. The nearly constant monovalent element partition coefficients are partially due to their weak dependence on temperature and composition (cf. smaller coefficients in

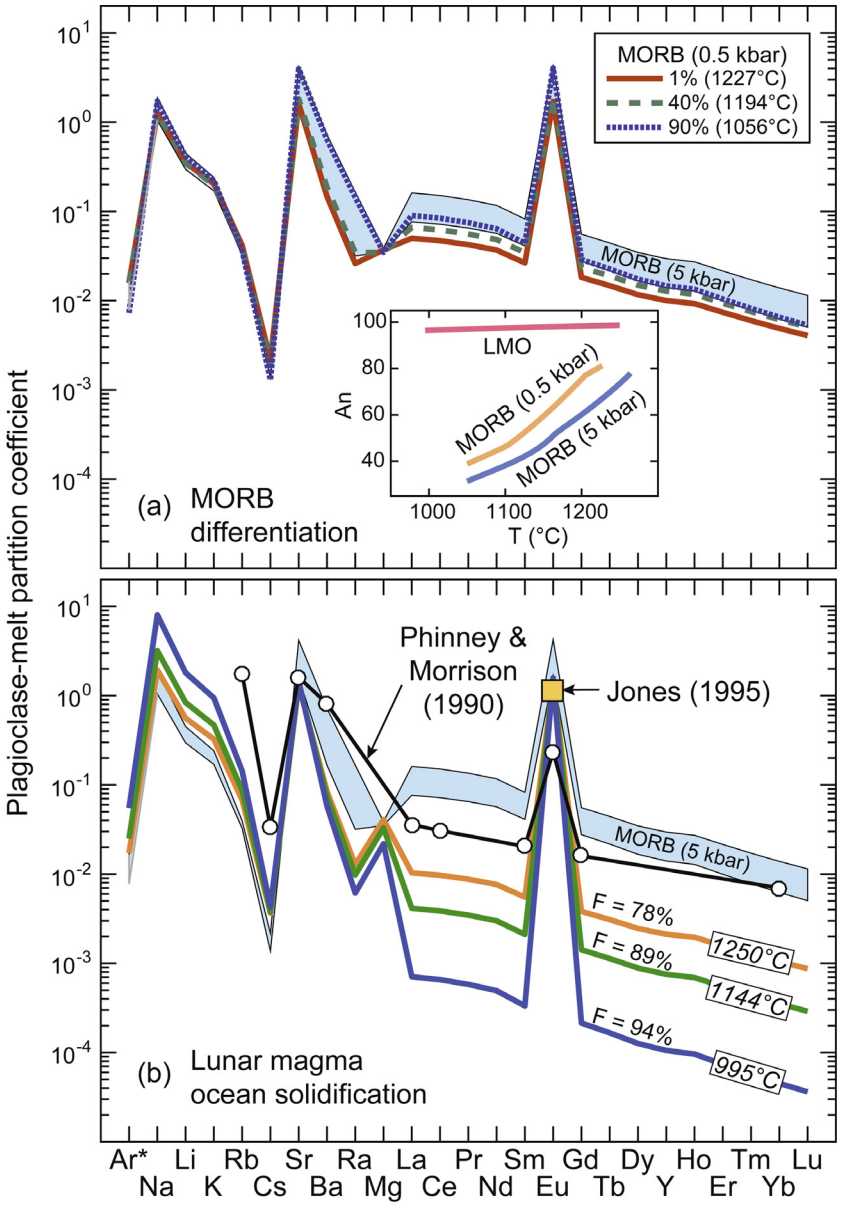

Fig. 11. Spider diagrams showing the calculated plagioclase-melt partition coefficients for fractional crystallization of a primary MORB (a) and a global lunar magma ocean (b). Inset in (a) illustrates the variations of anorthite content in plagioclase as a function of temperature. Ar^* denotes the calculated noble gas partition coefficients. See text for details.

Eq. (8a) than those in Eq. (6a)) as well as the competing effect between the two. As a result of systematically lower anorthite contents in plagioclase at the same temperatures, the calculated REE partition coefficients for the high-pressure crystallization are about a factor of two greater than those for the low-pressure case. Therefore, for noble gases, monovalent elements, and REE, constant plagioclase-melt partition coefficients could be used to approximately model chemical fractionation during MORB crystallization at a given pressure.

The predicted partition coefficients of divalent elements (Sr Ba, Ra, and Eu) for the two cases of MORB crystallization (0.5 kbar and 5 kbar) are comparable, but both become a factor of three to five larger throughout the crystallization processes. This is due to their similar variations of plagioclase anorthite contents (see inset in Fig. 11a), which is the primary factor controlling divalent element partitioning (Eq. (7a)). Given the non-negligible variations of divalent element partition coefficients, composition-dependent plagioclase-melt partition coefficients are required to quantify divalent element fractionation during MORB differentiation. This point is consistent with the modeling results in Blundy and Wood (1991) for Sr fractionation during plagioclase crystallization. On the contrary, Mg partition coefficients appear to be constant (0.036 ± 0.001) during MORB crystallization at both pressures because of the competition between r_0 and E (see Eqs. (7b) and (7c)). For the convenience of interested readers,

Table 3
Plagioclase-melt trace element partition coefficients at representative crystallization stages of primary mid-ocean ridge basalt and lunar magma ocean.

	MORB[a] (0.5 kbar)			MORB[a] (5 kbar)			LMO[b]			
F (%)[c]	1	40	90	13	76	96	78	89	94	[d]
An (mol%)	81.3	73.4	39.7	77.9	58.7	32.2	98.7	97.9	96.4	98.7
T (°C)/P (kbar)	1227/0.5	1194/0.5	1056/0.5	1264/5	1194/5	1056/5	1250/4.6	1144/2	995/1	1350/4.6
Ar*[e]	0.017	0.017	0.007	0.019	0.013	0.009	0.028	0.046	0.146	0.015
Na	1.28	1.28	1.76	1.12	1.10	1.96	2.24	3.87	11.04	1.27
K	0.22	0.21	0.24	0.20	0.18	0.26	0.39	0.59	1.35	0.25
Li	0.37	0.36	0.44	0.34	0.31	0.49	0.66	1.05	2.57	0.41
Rb	0.046	0.042	0.041	0.043	0.036	0.045	0.084	0.113	0.213	0.058
Cs	0.0025	0.0022	0.0015	0.0025	0.0019	0.0017	0.0048	0.0053	0.0069	0.0040
Ca	1.37	1.44	2.35	1.32	1.60	2.38	1.31	1.38	1.44	1.29
Sr	1.61	1.83	4.16	1.59	2.31	4.30	1.29	1.37	1.45	1.27
Ba	0.147	0.185	0.640	0.164	0.307	0.700	0.086	0.076	0.060	0.100
Mg	0.037	0.035	0.036	0.038	0.037	0.036	0.040	0.033	0.022	0.049
Ra	0.026	0.034	0.140	0.031	0.065	0.157	0.013	0.010	0.006	0.017
La	5.01E−02	6.62E−02	9.03E−02	7.65E−02	1.43E−01	9.19E−02	1.03E−02	4.14E−03	7.08E−04	2.70E−02
Ce	4.70E−02	6.20E−02	8.39E−02	7.18E−02	1.34E−01	8.55E−02	9.70E−03	3.87E−03	6.57E−04	2.54E−02
Pr	4.24E−02	5.58E−02	7.48E−02	6.50E−02	1.20E−01	7.62E−02	8.77E−03	3.47E−03	5.82E−04	2.32E−02
Nd	3.69E−02	4.84E−02	6.39E−02	5.68E−02	1.04E−01	6.51E−02	7.65E−03	3.00E−03	4.93E−04	2.04E−02
Sm	2.65E−02	3.45E−02	4.39E−02	4.11E−02	7.43E−02	4.48E−02	5.52E−03	2.11E−03	3.33E−04	1.50E−02
Eu^{2+}	1.70	1.92	4.25	1.67	2.39	4.39	1.38	1.47	1.57	1.35
Gd	1.82E−02	2.36E−02	2.89E−02	2.85E−02	5.07E−02	2.94E−02	3.82E−03	1.42E−03	2.14E−04	1.06E−02
Tb	1.47E−02	1.89E−02	2.27E−02	2.31E−02	4.07E−02	2.31E−02	3.09E−03	1.13E−03	1.66E−04	8.70E−03
Dy	1.17E−02	1.49E−02	1.74E−02	1.84E−02	3.21E−02	1.77E−02	2.46E−03	8.85E−04	1.26E−04	7.02E−03
Y	1.00E−02	1.28E−02	1.47E−02	1.59E−02	2.75E−02	1.49E−02	2.12E−03	7.53E−04	1.06E−04	6.10E−03
Ho	9.26E−03	1.18E−02	1.34E−02	1.47E−02	2.54E−02	1.37E−02	1.96E−03	6.93E−04	9.62E−05	5.67E−03
Er	7.40E−03	9.37E−03	1.04E−02	1.18E−02	2.02E−02	1.06E−02	1.57E−03	5.47E−04	7.38E−05	4.61E−03
Tm	5.98E−03	7.53E−03	8.19E−03	9.60E−03	1.62E−02	8.34E−03	1.27E−03	4.36E−04	5.73E−05	3.78E−03
Yb	4.89E−03	6.13E−03	6.53E−03	7.89E−03	1.32E−02	6.65E−03	1.04E−03	3.53E−04	4.52E−05	3.14E−03
Lu	4.06E−03	5.08E−03	5.30E−03	6.59E−03	1.09E−02	5.40E−03	8.71E−04	2.90E−04	3.63E−05	2.65E−03

[a] Isobaric fractional crystallization of MORB calculated using the MELTS program (Ghiorso et al., 2002; Smith and Asimow, 2005), a primary mid-ocean ridge basalt (MORB) composition from Workman and Hart (2005), and two choices of pressures (0.5 and 5 kbar).

[b] Fractional crystallization of lunar magma ocean (LMO) calculated using the MAGFOX program of Longhi (1992), a lunar upper mantle composition from Longhi (2006), and an initial pressure of 4 GPa.

[c] The degrees of solidification.

[d] Partition coefficients for the first plagioclases in LMO at a hypothetical higher crystallization temperature (1350 °C).

[e] The estimated plagioclase-melt noble gas partition coefficients.

the calculated plagioclase-melt trace element partition coefficients are summarized in Table 3 for three representative An and temperatures during MORB crystallization at 0.5 kbar and 5 kbar.

5.3.2. Lunar magma ocean solidification

Fractional crystallization of a global lunar magma ocean was calculated using the MAGFOX program (Longhi, 1992, 2006) for a lunar upper mantle composition (LPUM; Longhi, 2006). Anorthitic plagioclase (An = 98.6) begins to crystalize at 78% solidification of the LMO at 1250 °C and 4.6 kbar. As crystallization proceeds, the anorthite content in plagioclase slightly decreases by only ~2 mol% with a ~250 °C decrease in the crystallization temperature (see inset in Fig. 11a). Using the newly parameterized partitioning models, we calculated plagioclase-melt partition coefficients for three representative stages of LMO crystallization (F): plagioclase saturation ($F = 78\%$, at 1250 °C and 4.6 kbar), spinel saturation ($F = 89\%$, at 1144 °C and 2.0 kbar), and the maximum extent solidification of MAGFOX's capability ($F = 94\%$, at 995 °C and 1.0 kbar). The results are shown in Fig. 11b and listed in Table 3.

The divalent element (Sr, Ba, Ra, and Eu^{2+}) partition coefficients display small changes across the 250 °C temperature range, because of the strong dependence on Ca content in plagioclase (Eq. (7a)) and the nearly invariant plagioclase composition; however, the small increase of albite content in plagioclase gives rise to a slightly larger r_0 and hence about a factor of two decrease in Mg partition coefficients. As crystallization proceeds from 78% to 94%, the predicted noble gas partition coefficient increases by a factor of three, monovalent element partition coefficients increase by a factor of three to four, and REE partition coefficients decrease by 1.5 orders of magnitude. Given the nearly invariant anorthite content in plagioclase, these variations mainly result from the 250 °C temperature range. Together with our recent study on REE partitioning in low-Ca pyroxene (Sun and Liang, 2013a), the large variations of plagioclase-melt partition coefficients of REE and monovalent elements underscore the importance of temperature and composition in quantifying trace element fractionation during LMO solidification.

Because the lunar interior likely has a very reduced oxidation state (about 1 log-unit below the iron-wüstite buffer; e.g., Papike et al., 2005), Eu would have been preferentially present as divalent cations (e.g., Drake, 1975; McKay et al., 1994) during LMO solidification, and therefore the Eu^{2+} partition coefficients can approximate Eu partition coefficients (or their upper limits) during anorthite fractionation in LMO. Interestingly, the estimated plagioclase-melt Eu^{2+} partition coefficients (0.85–0.91) are comparable to the Eu partition coefficients (1.15 in Jones, 1995; 1.0 in Weill and McKay, 1975) that have been used for estimating the parental magmas of lunar cumulate rocks. Compared with the phenocryst-matrix partitioning data from Phinney and Morrison (1990), the calculated REE partition coefficients for the first plagioclase crystals in LMO are a factor of four to seven smaller, and those for the subsequent plagioclases are up to about 2.5 orders of magnitude less. The estimated

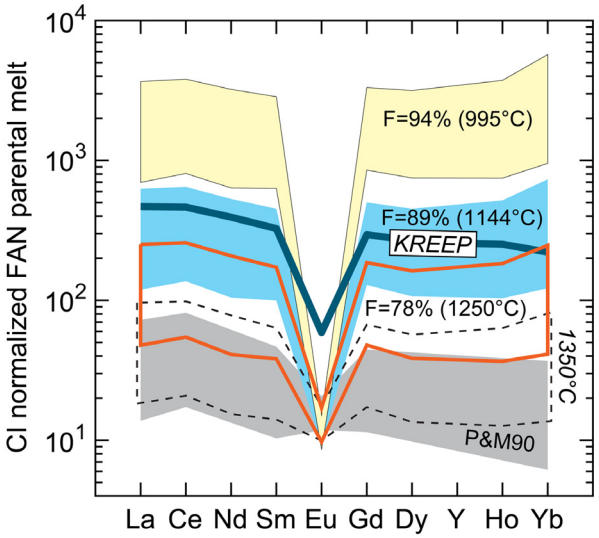

Fig. 12. Spider diagram showing the chondrite normalized REE abundances in the parental magmas of lunar ferroan anorthosites. The parental magmas were calculated using REE abundances in anorthite reported in Papike et al. (1997) and Floss et al. (1998) and partition coefficients from Phinney and Morrison (1990) and model calculations for three stages of lunar magma ocean solidification (78%, 89%, 94%) and a hypothetical high crystallization temperature (1350 °C). The model derived partition coefficients are listed in Table 3. Chondrite values are from Anders and Grevesse (1989). KREEP compositions are from Warren (1989).

Rb, Cs, and Ba partition coefficients for LMO plagioclases are about one order of magnitude less than those from Phinney and Morrison (1990), while the Sr partition coefficients are smaller. Hence, previous estimations of Eu abundances in FAN parental magmas (Papike et al., 1997; Floss et al., 1998) likely remain valid, while those of other trace elements involve significant underestimations.

Using the anorthite-melt partitioning data derived from LMO solidification (78%, 89% and 94%; Table 3), we reassessed the parental magmas of FANs with reported anorthite REE data from the literature (i.e., Papike et al., 1997; Floss et al., 1998). Fig. 12 displays the estimated parental magma compositions. For each set of REE partition coefficients, the estimated REE abundances vary by a factor of five, which may be attributed to different extents of LMO solidification (e.g., Papike et al., 1997; Floss et al., 1998) and partially to subsolidus re-equilibration. The partition coefficients derived from LMO solidification give rise to Eu abundances comparable to previous estimations (~20 time chondrite values). Because of the systematic decreases of REE partition coefficients during LMO solidification, the estimated REE abundances in the parental magmas appear to increase from 100 to 2000 times chondrite values with increasing Eu negative anomalies. Interestingly, the REE compositions of FAN parental magmas calculated using the partition coefficients at 89% LMO solidification are comparable to those of the KREEP basalts (K, REE, and P rich; Warren, 1989).

The anomalous REE enrichments and apparent Eu negative anomalies in FAN parental magmas may be due to

inappropriate temperatures used for partition coefficient calculations. As shown in Fig. 11, temperature primarily determines anorthite-melt REE partition coefficients during LMO solidification and hence estimations of REE abundances in the FAN parental magmas. Assuming a higher temperature (1350 °C) of FAN crystallization, we calculated a new set of anorthite-melt REE partition coefficients using the composition of the first LMO plagioclase crystals (An = 98.6) and Eqs. ((3) and (6a)–(6c)). REE abundances in the parental magmas become more comparable to previous estimations and display flat patterns without significant Eu anomalies (see dashed outline in Fig. 12). Thus, the determination of FAN crystallization temperatures is prerequisite for estimating their parental magmas and further assessing formation of the lunar crust.

6. SUMMARY AND CONCLUSIONS

We measured trace element partition coefficients between anorthite and a lunar high-Ti picritic melt and between anorthitic plagioclase and a MORB melt at 0.6 GPa and 1350–1400 °C. Using these new partitioning data and those from the literature, we developed new parameterized lattice strain models for the partitioning of monovalent (Na, K, Li), divalent (Ca, Mg, Sr, Ba, Ra), and trivalent (REE and Y) elements between plagioclase and silicate melt. Our models demonstrate that the temperature effect is small to negligible for monovalent and divalent element partitioning, but is important for trivalent element partitioning in plagioclase. A weak pressure effect also appears significant for the partitioning of all three groups of elements, although more high-pressure laboratory experiments are needed to further examine this effect.

Applying these models to phenocrysts with equilibrium melts reported in the literature, we showed that these models could be extrapolated to hydrous conditions (H_2O = ~0.6–4 wt%), low An (= 29) plagioclase, and high SiO_2 (= 66%) melt. In addition, a companion study (Sun and Liang, 2017) further demonstrated that the new REE partitioning model for plagioclase-melt is internally consistent with our previous model for clinopyroxene-melt (Sun and Liang, 2012), which allows the development of a new thermometer based on REE partitioning between plagioclase and clinopyroxene. Our new plagioclase-melt trace element partitioning models can also predict Ra and Ba partition coefficients for Ra-Th dating on plagioclase phenocrysts. Combining these models with the electrostatic model, we derived the first predictive model for plagioclase-melt noble gas partitioning.

Our new models are broadly applicable to terrestrial and lunar magmatism involving plagioclase crystallization over a wide range of temperature and pressure. During isobaric fractional crystallization of MORB, the competing effects of temperature and plagioclase composition leads to small variations of noble gas, monovalent and trivalent cation partition coefficients, while divalent cation partition coefficients display moderate variations primarily due to the composition changes. Although pressure is not the primary factor controlling trivalent element partitioning, a higher pressure systematically decreases Ca content in plagioclase at a given temperature, which effectively increases trivalent element partition coefficients.

However, during LMO solidification, the nearly invariant plagioclase composition accompanied by a significant temperature decrease leads to nearly constant divalent element partition coefficients and moderate variations in noble gas and monovalent element partition coefficients. The temperature decrease is particularly important for REE fractionation in the LMO as it reduces the partition coefficients by 1.5 orders of magnitude. Using the anorthite-melt partition coefficients at different stages (equivalent to different temperatures) of LMO solidification, the estimated REE abundances in the FAN parental magmas vary over one order of magnitude with significant Eu negative anomalies. Thus, estimations of FAN parental magma compositions strongly depend on how well the crystallization temperatures can be constrained.

ACKNOWLEDGEMENTS

We thank Marion Lytle and Soumen Mallick for their help and advice in LA-ICP-MS analysis, and Joe Boesenberg for his assistance in microprobe analyses. Wim van Westrenen shared unpublished manuscript and is greatly appreciated. Thoughtful reviews by the Associate Editor Mike Toplis, Ralf Dohmen and an anonymous reviewer helped to improve this manuscript. C. Sun acknowledges support from the Devonshire postdoctoral scholarship at WHOI. Our work on trace element partitioning in major rock-forming minerals has been supported by grants from NSF and NASA, most recently through EAR-1632815, NNX13AH07G and NNX16AR96G.

APPENDIX A. SUPPLEMENTARY MATERIAL

Supplementary data associated with this article can be found, in the online version, at http://dx.doi.org/10.1016/j.gca.2017.03.003.

REFERENCES

Aigner-Torres M., Blundy J., Ulmer P. and Pettke T. (2007) Laser Ablation ICPMS study of trace element partitioning between plagioclase and basaltic melts: an experimental approach. *Contrib. Mineral. Petrol.* **153**, 647–667.

Anders E. and Grevesse N. (1989) Abundances of the elements: meteoritic and solar. *Geochim. Cosmochim. Acta* **53**, 197–214.

Angel R. J. (2004) Equations of state of plagioclase feldspars. *Contrib. Mineral. Petrol.* **146**, 506–512.

Bédard J. H. (2006) Trace element partitioning in plagioclase feldspar. *Geochim. Cosmochim. Acta* **70**, 3717–3742.

Benusa M. D., Angel R. J. and Ross N. L. (2005) Compression of albite, $NaAlSi_3O_8$. *Am. Mineral.* **90**, 1115–1120.

Bindeman I. N. and Davis A. M. (2000) Trace element partitioning between plagioclase and melt: investigation of dopant influence on partition behavior. *Geochim. Cosmochim. Acta* **64**, 2863–2878.

Bindeman I. N., Davis A. M. and Drake M. J. (1998) Ion microprobe study of plagioclase-basalt partition experiments at natural concentration levels of trace elements. *Geochim. Cosmochim. Acta* **62**, 1175–1193.

Blundy J. (1997) Experimental study of a Kiglapait marginal rock and implications for trace element partitioning in layered intrusions. *Chem. Geol.* **141**, 73–92.

Blundy J. and Wood B. (1994) Prediction of crystal-melt partition coefficients from elastic moduli. *Nature* **372**, 452–454.

Blundy J. D. and Wood B. J. (1991) Crystal-chemical controls on the partitioning of Sr and Ba between plagioclase feldspar, silicate melts, and hydrothermal solutions. *Geochim. Cosmochim. Acta* **55**, 193–209.

Blundy J. D. and Wood B. J. (2003) Mineral-melt partitioning of uranium, thorium and their daughters. *Rev. Mineral. Geochem.* **52**, 59–123.

Blundy J. D., Robinson J. A. C. and Wood B. J. (1998) Heavy REE are compatible in clinopyroxene on the spinel lherzolite solidus. *Earth Planet. Sci. Lett.* **160**(3), 493–504.

Brice J. C. (1975) Some thermodynamic aspects of the growth of strained crystals. *J. Cryst. Growth* **28**(2), 249–253.

Broadhurst C. L., Drake M. J., Hagee B. E. and Bernatowicz T. J. (1990) Solubility and partitioning of Ar in anorthite, diopside, forsterite, spinel, and synthetic basaltic liquids. *Geochim. Cosmochim. Acta* **54**, 299–309.

Brooker R. A., Du Z., Blundy J. D., Kelley S. P., Allan N. L., Wood B. J., Chamorro E. M., Wartho J. A. and Purton J. A. (2003) The 'zero charge'partitioning behaviour of noble gases during mantle melting. *Nature* **423**, 738–741.

Carroll M. R., Draper D. S., Brooker R. A. and Kelley S. (1994) Noble gas solubilities in melts and crystals. *Noble Gas Geochem. Cosmochem.*, 325–341.

Cherniak D. J. (2010) Cation diffusion in feldspars. *Rev. Mineral. Geochem.* **72**, 691–733.

Cooper K. M. and Reid M. R. (2003) Re-examination of crystal ages in recent Mount St. Helens lavas: implications for magma reservoir processes. *Earth Planet. Sci. Lett.* **213**, 149–167.

Cooper K. M., Reid M. R., Murrell M. T. and Clague D. A. (2001) Crystal and magma residence at Kilauea Volcano, Hawaii: ^{230}Th–^{226}Ra dating of the 1955 east rift eruption. *Earth Planet. Sci. Lett.* **184**, 703–718.

Curetti N., Sochalski-Kolbus L. M., Angel R. J., Benna P., Nestola F. and Bruno E. (2011) High-pressure structural evolution and equation of state of analbite. *Am. Mineral.* **96**, 383–392.

de Vries J., van Westrenen W. and van den Berg A. (2012) Radiogenic heat production in the Moon: constraints from plagioclase-melt trace element partitioning experiments. *Lunar Planet. Sci. Conf.* **43**, 1737.

Dick H. J. B., Natland J. H., Alt J. C., Bach W., Bideau D., Gee J. S., Haggas S., Hertogen J. G. H., Hirth G., Holm P. M., Ildefonse B., Iturrino G. J., John B. E., Kelley D. S., Kikawa E., Kingdon A., LeRoux P. J., Maeda J., Meyer P. S., Miller D. J., Naslund H. R., Niu Y.-L., Robinson P. T., Snow J., Stephen R. A., Trimby P. W., Worm H.-U. and Yoshinobu A. (2000) A long in situ section of the lower ocean crust: results of ODP Leg 176 drilling at the Southwest Indian Ridge. *Earth Planet. Sci. Lett.* **179**, 31–51.

Dohmen R. and Blundy J. (2014) A predictive thermodynamic model for element partitioning between plagioclase and melt as a function of pressure, temperature and composition. *Am. J. Sci.* **314**, 1319–1372.

Drake M. J. (1975) The oxidation state of europium as an indicator of oxygen fugacity. *Geochim. Cosmochim. Acta* **39**, 55–64.

Drake M. J. and Weill D. F. (1975) Partition of Sr, Ba, Ca, Y, Eu^{2+}, Eu^{3+}, and other REE between plagioclase feldspar and magmatic liquid: an experimental study. *Geochim. Cosmochim. Acta* **39**, 689–712.

Dygert N., Liang Y., Sun C. and Hess P. (2014) An experimental study of trace element partitioning between augite and Fe-rich basalts. *Geochim. Cosmochim. Acta* **132**, 170–186.

Fabbrizio A., Schmidt M. W., Günther D. and Eikenberg J. (2009) Experimental determination of Ra mineral/melt partitioning for feldspars and 226 Ra-disequilibrium crystallization ages of plagioclase and alkali-feldspar. *Earth Planet. Sci. Lett.* **280**, 137–148.

Fedele L., Lustrino M., Melluso L., Morra V., Zanetti A. and Vannucci R. (2015) Trace-element partitioning between plagioclase, alkali feldspar, Ti-magnetite, biotite, apatite, and evolved potassic liquids from Campi Flegrei (Southern Italy). *Am. Mineral.* **100**, 233–249.

Floss C., James O. B., McGee J. J. and Crozaz G. (1998) Lunar ferroan anorthosite petrogenesis: clues from trace element distributions in FAN subgroups. *Geochim. Cosmochim. Acta* **62**, 1255–1283.

Frei D., Liebscher A., Franz G., Wunder B., Klemme S. and Blundy J. (2009) Trace element partitioning between orthopyroxene and anhydrous silicate melt on the lherzolite solidus from 1.1 to 3.2 GPa and 1230 to 1535 °C in the model system Na_2O-CaO-MgO-Al_2O_3-SiO_2. *Contrib. Mineral. Petrol.* **157**, 473–490.

Gaetani G. A. and Grove T. L. (1995) Partitioning of rare earth elements between clinopyroxene and silicate melt crystal-chemical controls. *Geochim. Cosmochim. Acta* **59**(10), 1951–1962.

Ghiorso M. S., Hirschmann M. M., Reiners P. W. and Kress V. C. (2002) The pMELTS: a revision of MELTS for improved calculation of phase relations and major element partitioning related to partial melting of the mantle to 3 GPa. *Geochem., Geophys., Geosyst.* **3**. http://dx.doi.org/10.1029/2001GC000217.

Gross J., Treiman A. H. and Mercer C. N. (2014) Lunar feldspathic meteorites: constraints on the geology of the lunar highlands, and the origin of the lunar crust. *Earth Planet. Sci. Lett.* **388**, 318–328.

Hazen R. M. and Finger L. W. (1979) Bulk modulus–volume relationship for cation-anion polyhedra. *J. Geophys. Res.: Solid Earth* **84**, 6723–6728.

Heber V. S., Brooker R. A., Kelley S. P. and Wood B. J. (2007) Crystal–melt partitioning of noble gases (helium, neon, argon, krypton, and xenon) for olivine and clinopyroxene. *Geochim. Cosmochim. Acta* **71**, 1041–1061.

Hill E., Blundy J. D. and Wood B. J. (2011) Clinopyroxene–melt trace element partitioning and the development of a predictive model for HFSE and Sc. *Contrib. Mineral. Petrol.* **161**, 423–438.

Hill E., Wood B. J. and Blundy J. D. (2000) The effect of Ca-Tschermaks component on trace element partitioning between clinopyroxene and silicate melt. *Lithos* **53**, 203–215.

Holland T. and Powell R. (1992) Plagioclase feldspars; activity-composition relations based upon Darken's quadratic formalism and Landau theory. *Am. Mineral.* **77**, 53–61.

Hui H., Oshrin J. G. and Neal C. R. (2011) Investigation into the petrogenesis of Apollo 14 high-Al basaltic melts through crystal stratigraphy of plagioclase. *Geochim. Cosmochim. Acta* **75**, 6439–6460.

Jackson C. R., Parman S. W., Kelley S. P. and Cooper R. F. (2013) Constraints on light noble gas partitioning at the conditions of spinel-peridotite melting. *Earth Planet. Sci. Lett.* **384**, 178–187.

Jones J. H. (1995) Experimental trace element partitioning. Rock Physics and Phase Relations: A Handbook of Physical Constants, pp. 73-104.

Kneip H. J. and Liebau F. (1994) Feldspars with trivalent non-tetrahedral cations: Experimental studies in the system $NaAlSi_3O_8$-$CaAl_2Si_2O_8$-$LaAl_3SiO_8$. *Euro. J. Mineral.* **6**, 87–98.

Lange R. A., Frey H. M. and Hector J. (2009) A thermodynamic model for the plagioclase-liquid hygrometer/thermometer. *Am. Mineral.* **94**, 494–506.

Laubier M., Grove T. L. and Langmuir C. H. (2014) Trace element mineral/melt partitioning for basaltic and basaltic andesitic melts: an experimental and laser ICP-MS study with application to the oxidation state of mantle source regions. *Earth Planet. Sci. Lett.* **392**, 265–278.

Lissenberg C. J., MacLeod C. J., Howard K. A. and Godard M. (2013) Pervasive reactive melt migration through fast-spreading lower oceanic crust (Hess Deep, equatorial Pacific Ocean). *Earth Planet. Sci. Lett.* **361**, 436–447.

Longhi J. (1992) Origin of picritic green glass magmas by polybaric fractional fusion. *Lunar Planet. Sci. Conf. Proc.* **22**, 343–353.

Longhi J. (2006) Petrogenesis of picritic mare magmas: constraints on the extent of early lunar differentiation. *Geochim. Cosmochim. Acta* **70**, 5919–5934.

Longhi J., Walker D. and Hays J. F. (1976) Fe and Mg in plagioclase. *Lunar Planet. Sci. Conf. Proc.* **7**, 1281–1300.

Lundstrom C. C., Shaw H. F., Ryerson F. J., Williams Q. and Gill J. (1998) Crystal chemical control of clinopyroxene-melt partitioning in the Di-Ab-An system: implications for elemental fractionations in the depleted mantle. *Geochim. Cosmochim. Acta* **62**, 2849–2862.

Marianelli P., Sbrana A. and Proto M. (2006) Magma chamber of the Campi Flegrei supervolcano at the time of eruption of the Campanian Ignimbrite. *Geology* **34**, 937–940.

McGee J. J. (1993) Lunar ferroan anorthosites: mineralogy, compositional variations, and petrogenesis. *J. Geophys. Res.* **98**, 9089–9105.

McKay G. A. (1982) Partitioning of REE between olivine, plagioclase, and synthetic basaltic melts: implications for the origin of lunar anorthosites. *Lunar Planet. Sci. Conf.* **13**, 493–494.

McKay G., Le L., Wagstaff J. and Crozaz G. (1994) Experimental partitioning of rare earth elements and strontium: constraints on petrogenesis and redox conditions during crystallization of Antarctic angrite Lewis Cliff 86010. *Geochim. Cosmochim. Acta* **58**, 2911–2919.

Miller S. A., Asimow P. D. and Burnett D. S. (2006) Determination of melt influence on divalent element partitioning between anorthite and CMAS melts. *Geochim. Cosmochim. Acta* **70**, 4258–4274.

Miller S. A., Burnett D. S., Asimow P. D., Phinney D. L. and Hutcheon I. D. (2007) Experimental study of radium partitioning between anorthite and melt at 1 atm. *Am. Mineral.* **92**, 1535–1538.

Mollo S., Putirka K., Iezzi G., Del Gaudio P. and Scarlato P. (2011) Plagioclase–melt (dis) equilibrium due to cooling dynamics: implications for thermometry, barometry and hygrometry. *Lithos* **125**, 221–235.

Namur O., Charlier B., Toplis M. J. and Vander Auwera. J. (2012) Prediction of plagioclase-melt equilibria in anhydrous silicate melts at 1-atm. *Contrib. Mineral. Petrol.* **163**, 133–150.

Onuma N., Higuchi H., Wakita H. and Nagasawa H. (1968) Trace element partition between two pyroxenes and the host lava. *Earth Planet. Sci. Lett.* **5**, 47–51.

Papike J. J., Fowler G. W. and Shearer C. K. (1997) Evolution of the lunar crust: SIMS study of plagioclase from ferroan anorthosites. *Geochim. Cosmochim. Acta* **61**, 2343–2350.

Papike J. J., Fowler G. W., Shearer C. K. and Layne G. D. (1996) Ion microprobe investigation of plagioclase and orthopyroxene from lunar Mg-suite norites: implications for calculating parental melt REE concentrations and for assessing postcrystallization REE redistribution. *Geochim. Cosmochim. Acta* **60**, 3967–3978.

Papike J. J., Karner J. M. and Shearer C. K. (2005) Comparative planetary mineralogy: valence state partitioning of Cr, Fe, Ti, and V among crystallographic sites in olivine, pyroxene, and spinel from planetary basalts. *Am. Mineral.* **90**(2–3), 277–290.

Papike J. J., Ryder G. and Shearer C. K. (1998) Lunar samples. *Rev. Mineral. Geochem.* **36**, 5-1.

Peters M. T., Shaffer E. E., Burnett D. S. and Kim S. S. (1995) Magnesium and titanium partitioning between anorthite and Type B CAI liquid: dependence on oxygen fugacity and liquid composition. *Geochim. Cosmochim. Acta* **59**, 2785–2796.

Phinney W. C. and Morrison D. A. (1990) Partition coefficients for calcic plagioclase: implications for Archean anorthosites. *Geochim. Cosmochim. Acta* **54**, 1639–1654.

Putirka K. D. (2005) Igneous thermometers and barometers based on plagioclase+ liquid equilibria: tests of some existing models and new calibrations. *Am. Mineral.* **90**, 336–346.

Seber G. and Wild C. (1989) *Nonlinear Regression*. Wiley, New York.

Severs M. J., Beard J. S., Fedele L., Hanchar J. M., Mutchler S. R. and Bodnar R. J. (2009) Partitioning behavior of trace elements between dacitic melt and plagioclase, orthopyroxene, and clinopyroxene based on laser ablation ICPMS analysis of silicate melt inclusions. *Geochim. Cosmochim. Acta* **73**, 2123–2141.

Shannon R. T. (1976) Revised effective ionic radii and systematic studies of interatomic distances in halides and chalcogenides. *Acta Crystall. Sect. A: Cryst. Phys., Diff., Theoret. Gen. Crystal.* **32**, 751–767.

Shearer C. K., Elardo S. M., Petro N. E., Borg L. E. and McCubbin F. M. (2015) Origin of the lunar highlands Mg-suite: an integrated petrology, geochemistry, chronology, and remote sensing perspective. *Am. Mineral.* **100**, 294–325.

Shervais J. W. and McGee J. J. (1998) Ion and electron microprobe study of troctolites, norite, and anorthosites from Apollo 14: Evidence for urKREEP assimilation during petrogenesis of Apollo 14 Mg-suite rocks. *Geochim. Cosmochim. Acta* **62**, 3009–3023.

Shimizu K. (2016) *Volatile Content of the Earth's Upper Mantle and Roles of Hydrous Phases in Igneous Processes* (Ph.D. thesis). Brown University.

Smith J. V., Anderson A. T., Newton R. C., Olsen E. J., Crewe A. V., Isaacson M. S., Johnson D. and Wyllie P. J. (1970) Petrologic history of the moon inferred from petrography, mineralogy and petrogenesis of Apollo 11 rocks. In: Proceedings of the Apollo 11 Lunar Science Conference, pp. 897–925.

Smith P. M. and Asimow P. D. (2005) Adiabat_1ph: a new public front-end to the MELTS, pMELTS, and pHMELTS models. *Geochem., Geophys., Geosyst.* **6**, Q02004. http://dx.doi.org/10.1029/2004GC000816.

Snyder G. A., Taylor L. A. and Neal C. R. (1992) A chemical model for generating the sources of mare basalts: combined equilibrium and fractional crystallization of the lunar magmasphere. *Geochim. Cosmochim. Acta* **56**, 3809–3823.

Stebbins J. F., Weill D. F., Carmichael I. S. E. and Moret L. K. (1982) High temperature heat contents and heat capacities of liquids and glasses in the system $NaAlSi_3O_8$-$CaAl_2Si_2O_8$. *Contrib. Mineral. Petrol.* **80**, 276–284.

Sun C. and Liang Y. (2012) Distribution of REE between clinopyroxene and basaltic melt along a mantle adiabat: effects of major element composition, water, and temperature. *Contrib. Mineral. Petrol.* **163**, 807–823.

Sun C. and Liang Y. (2013a) Distribution of REE and HFSE between low-Ca pyroxene and lunar picritic melts around multiple saturation points. *Geochim. Cosmochim. Acta* **119**, 340–358.

Sun C. and Liang Y. (2013b) The importance of crystal chemistry on REE partitioning between mantle minerals (garnet, clinopy-

roxene, orthopyroxene, and olivine) and basaltic melts. *Chem. Geol.* **358**, 23–36.

Sun C. and Liang Y. (2017) A REE-in-plagioclase-clinopyroxene thermometer for crustal rocks. *Contrib. Mineral. Petrol.*. http://dx.doi.org/10.1007/s00410-016-1326-9.

Tenner T. J., Lange R. A. and Downs R. T. (2007) The albite fusion curve re-examined: new experiments and the high-pressure density and compressibility of high albite and $NaAlSi_3O_8$ liquid. *Am. Mineral.* **92**, 1573–1585.

Tepley F. J., Lundstrom C. C., Gill J. B. and Williams R. W. (2006) U-Th-Ra disequilibria and the time scale of fluid transfer and andesite differentiation at Arenal volcano, Costa Rica (1968–2003). *J. Volcanol. Geotherm. Res.* **157**, 147–165.

Tepley F. J., Lundstrom C. C., McDonough W. F. and Thompson A. (2010) Trace element partitioning between high-An plagioclase and basaltic to basaltic andesite melt at 1 atmosphere pressure. *Lithos* **118**, 82–94.

van Westrenen W. and Draper D. S. (2007) Quantifying garnet-melt trace element partitioning using lattice-strain theory: new crystal-chemical and thermodynamic constraints. *Contrib. Mineral. Petrol.* **154**, 717–730.

van Westrenen W., Blundy J. and Wood B. (1999) Crystal-chemical controls on trace element partitioning between garnet and anhydrous silicate melt. *Am. Mineral.* **84**, 838–847.

van Westrenen W., Wood B. J. and Blundy J. D. (2001) A predictive thermodynamic model of garnet–melt trace element partitioning. *Contrib. Mineral. Petrol.* **142**, 219–234.

Volpe A. M. and Hammond P. E. (1991) ^{238}U–^{230}Th–^{226}Ra disequilibria in young Mount St. Helens rocks: time constraint for magma formation and crystallization. *Earth Planet. Sci. Lett.* **107**, 475–486.

Wardell L. J., Kyle P. R., Dunbar N. and Christenson B. (2001) White Island volcano, New Zealand: carbon dioxide and sulfur dioxide emission rates and melt inclusion studies. *Chem. Geol.* **177**, 187–200.

Warren P. H. (1985) The magma ocean concept and lunar evolution. *Ann. Rev. Earth Planet. Sci.* **13**, 201–240.

Warren P. H. (1989) KREEP: major-element diversity, trace-element uniformity (almost). In: Moon in Transition: Apollo 14, KREEP, and Evolved Lunar Rocks, vol. 1, pp. 149–153.

Weill D. F. and McKay G. A. (1975) The partitioning of magnesium, iron, strontium, cerium, samarium, europium, and ytterbium in lunar igneous systems and a possible origin of KREEP by equilibrium partial melting. In: Proceedings 6th Lunar Science Conference, pp. 1143–1158.

Weill D. F., Stebbins J. F., Hon R. and Carmichael I. S. E. (1980) The enthalpy of fusion of anorthite. *Contrib. Mineral. Petrol.* **74**, 95–102.

Wood B. J. and Blundy J. D. (1997) A predictive model for rare earth element partitioning between clinopyroxene and anhydrous silicate melt. *Contrib. Mineral. Petrol.* **129**, 166–181.

Wood B. J. and Blundy J. D. (2003) Trace element partitioning under crustal and uppermost mantle conditions: the influences of ionic radius, cation charge, pressure, and temperature. *Treat. Geochem.* **2**, 395–424.

Wood J. A., Dickey, Jr., J. S., Marvin U. B. and Powell B. N. (1970) Lunar anorthosites and a geophysical model of the moon. In: Proceedings of the Apollo 11 Lunar Science Conference, pp. 965–988.

Workman R. K. and Hart S. R. (2005) Major and trace element composition of the depleted MORB mantle (DMM). *Earth Planet. Sci. Lett.* **231**, 53–72.

Yao L., Sun C. and Liang Y. (2012) A parameterized model for REE distribution between low-Ca pyroxene and basaltic melts with applications to REE partitioning in low-Ca pyroxene along a mantle adiabat and during pyroxenite-derived melt and peridotite interaction. *Contrib. Mineral. Petrol.* **164**, 261–280.

Zajacz Z. and Halter W. (2007) LA-ICPMS analyses of silicate melt inclusions in co-precipitated minerals: quantification, data analysis and mineral/melt partitioning. *Geochim. Cosmochim. Acta* **71**, 1021–1040.

Zellmer G. F., Rubin K. H., Grönvold K. and Jurado-Chichay Z. (2008) On the recent bimodal magmatic processes and their rates in the Torfajökull-Veidivötn area, Iceland. *Earth Planet. Sci. Lett.* **269**, 388–398.

Associate Editor: Michael J. Toplis